J Neurophysiol 130: 86–103, 2023.
First published June 14, 2023; doi:10.1152/jn.00068.2022

american physiological society

JNP JOURNAL OF NEUROPHYSIOLOGY

RESEARCH ARTICLE

Computational Neuroscience

Rapid thalamocortical network switching mediated by cortical synchronization underlies propofol-induced EEG signatures: a biophysical model

Austin E. Soplata,[1,2]* Elie Adam,[3,4]* Emery N. Brown,[1,3,4,5] Patrick L. Purdon,[1] Michelle M. McCarthy,[2]* and Nancy Kopell[2]*

[1]*Department of Anesthesia, Critical Care and Pain Medicine, Massachusetts General Hospital, Harvard Medical School, Boston, Massachusetts, United States;* [2]*Department of Mathematics and Statistics, Boston University, Boston, Massachusetts, United States;* [3]*Department of Brain and Cognitive Sciences, Massachusetts Institute of Technology, Cambridge, Massachusetts, United States;* [4]*Picower Institute for Learning and Memory, Massachusetts Institute of Technology, Cambridge, Massachusetts, United States; and* [5]*Institute for Medical Engineering and Science, Massachusetts Institute of Technology, Cambridge, Massachusetts, United States*

Abstract

Propofol-mediated unconsciousness elicits strong alpha/low-beta and slow oscillations in the electroencephalogram (EEG) of patients. As anesthetic dose increases, the EEG signal changes in ways that give clues to the level of unconsciousness; the network mechanisms of these changes are only partially understood. Here, we construct a biophysical thalamocortical network involving brain stem influences that reproduces transitions in dynamics seen in the EEG involving the evolution of the power and frequency of alpha/low-beta and slow rhythm, as well as their interactions. Our model suggests that propofol engages thalamic spindle and cortical sleep mechanisms to elicit persistent alpha/low-beta and slow rhythms, respectively. The thalamocortical network fluctuates between two mutually exclusive states on the timescale of seconds. One state is characterized by continuous alpha/low-beta-frequency spiking in thalamus (C-state), whereas in the other, thalamic alpha spiking is interrupted by periods of co-occurring thalamic and cortical silence (I-state). In the I-state, alpha colocalizes to the peak of the slow oscillation; in the C-state, there is a variable relationship between an alpha/beta rhythm and the slow oscillation. The C-state predominates near loss of consciousness; with increasing dose, the proportion of time spent in the I-state increases, recapitulating EEG phenomenology. Cortical synchrony drives the switch to the I-state by changing the nature of the thalamocortical feedback. Brain stem influence on the strength of thalamocortical feedback mediates the amount of cortical synchrony. Our model implicates loss of low-beta, cortical synchrony, and coordinated thalamocortical silent periods as contributing to the unconscious state.

NEW & NOTEWORTHY GABAergic anesthetics induce alpha/low-beta and slow oscillations in the EEG, which interact in dose-dependent ways. We constructed a thalamocortical model to investigate how these interdependent oscillations change with propofol dose. We find two dynamic states of thalamocortical coordination, which change on the timescale of seconds and dose-dependently mirror known changes in EEG. Thalamocortical feedback determines the oscillatory coupling and power seen in each state, and this is primarily driven by cortical synchrony and brain stem neuromodulation.

alpha rhythms; cholinergic modulation; slow rhythms; synchrony; thalamus

INTRODUCTION

Unconsciousness mediated by GABAergic anesthetics, such as propofol and sevoflurane, is characterized by a presence of alpha/low-beta (8–20 Hz) and slow (0.5–2.0 Hz) oscillations in the electroencephalogram (EEG) (1–7). As effect site concentration (dose) is increased, the EEG shows less low-beta, lower-frequency alpha, less alpha power, and increased slow-wave power (3, 4, 7). The alpha (8–14 Hz) and slow oscillations are interdependent, and the level of interdependence

*M. M. McCarthy and N. Kopell contributed equally to this work. A. E. Soplata and E. Adam contributed equally to this work.
Correspondence: A. E. Soplata (austin.soplata@gmail.com).
Submitted 22 February 2022 / Revised 8 June 2023 / Accepted 8 June 2023

was found to indicate the level of unconsciousness (3). References 3, 4, 7, and 8 highlighted two states they called "peak-max" and "trough-max." These are two states in which the slow and alpha rhythms are coupled by phase-amplitude coupling (PAC). In peak-max, the amplitude of the alpha rhythm is maximal during the peak of the slow rhythm; in trough-max, the maximal alpha amplitude appears in the trough of the slow rhythm. The trough-max state appears close to the loss of consciousness (LOC), whereas the peak-max state occurs with deeper levels of propofol. However, during most of the time spent under propofol, the EEG does not reflect either of these states. This is shown in Fig. 1.

Anesthetics act on their molecular targets, and it is then through network mechanisms that they alter brain rhythms (1, 9). The network mechanisms underlying the EEG phenomena above remain unclear. Our previous work (10) suggests that alpha emerges from thalamus under propofol and can be modulated by an external source of slow oscillation such as that modeled in Refs. 11 and 12. Additionally, the alpha/slow peak-max increases as dose increases. However, our model was open-loop, where cortex provides feedforward input to thalamus without feedback. It is unknown what dynamics are possible under a closed-loop interaction. Yet this interaction is essential during unconsciousness, for instance, to explain the anteriorization of alpha oscillations (13). In this work, we develop a biophysical model of closed-loop thalamocortical interaction that explains all the dose-dependent EEG phenomena above and shows the importance of thalamocortical feedback. Our Hodgkin–Huxley-type model builds on Refs. 10–12 and 14 to incorporate influences of cortex, thalamus, and brain stem on EEG dynamics.

In this article, we use 8–12 Hz as the range for alpha rather than the 8–14 Hz range used in Refs. 3 and 4. We note that 8–12 Hz is the standard range for alpha in the cognitive literature (15, 16). In the present article we aim to explain, using our mathematical simulation, how propofol-induced EEG rhythms can lead to a loss of cognitive function by disrupting neuronal communication. Thus, we make a distinction between alpha (8–12 Hz) and low-beta (13–20 Hz).

We show that the dynamics on small space- and time-scales are highly complex: on each slow cycle, there is one of two network states, which can change after some indeterminate number of slow cycles. One of those states is called the "C-state" and is characterized by continuous ("C") alpha/low-beta oscillations in thalamus; the other state is called the "I-state," in which there is thalamic spiking at an alpha frequency interrupted ("I") by a time period within a slow oscillation cycle in which there is no thalamic activity. The I-state is highly related to what has been called peak-max, since the alpha activity is colocalized with the peak of the slow oscillation. The interaction of alpha, low-beta, and slow during the C-state is more variable than in the I-state, and the alpha portion includes what has previously been called trough-max. We show that the statistics of these states are dose-dependent, with higher doses of propofol corresponding to a larger percentage of the I-state. A significant finding of the work is that the statistics of the two states are strongly influenced by the synchrony of the cortical cells. Thus, the depth of anesthesia corresponds to the statistics of the I-states and C-states. Unconsciousness is associated with a prevalence of the I-state and thus a higher degree of cortical synchronization. Such increased synchronization has been reported experimentally (17). See DISCUSSION for more details.

Systemic administration of GABAergic anesthetics affects all structures in the brain, and the influence of these drugs on the brain stem can alter neuromodulatory systems (18). Our simulations show that when feedback from thalamus to cortex is potentiated because of these alterations, the synchronization of cortex is facilitated and makes the switch to the I-state more probable. Endogenous noise in the system facilitates switching back to the C-state. Our work suggests that cortical synchronization due to potentiated thalamic feedback resulting from neuromodulatory alterations is key in understanding the mechanism of GABAergic anesthetic-mediated unconsciousness. The loss of beta with increasing dose also has implications for loss of long-distance communication needed for consciousness.

METHODS

Model Design

Our Hodgkin–Huxley network, illustrated in Fig. 2*A*, consists of 100 cortical pyramidal dendritic (PYdr) compartments, 100 corresponding cortical pyramidal somatic/axonal (PYso) compartments, 20 cortical interneuron cells (INs), 20 thalamic thalamocortical cells (TCs), and 20 thalamic reticular neurons (TRNs). All equations and parameters used in the model are available in both Supplemental Data S2 and the model code (19, 20). The thalamic cells are identical to those used in Ref. 10 and therefore derived from Refs. 14 and 21, except that we used a population size of 20 for each cell class rather than 50 because of memory/RAM limitations. The cortical compartments and cells are implemented according to their original description in Ref. 11, except that we include a simple leak current in our PYdr compartments; we suspect that the original paper accidentally neglected to list this current. Although there are many cortical slow models to choose from (21–29), we use this particular K(Na)-based sleep slow cortical model (11) because of its simplicity, experimental basis (23), and effective utilization in other slow models (12, 30).

Model Connectivity

All connections are illustrated in Fig. 2*A* and available in both Supplemental Data S2 and the model mechanism code (20). AMPA connections include from PYso to neighbor-only PYdr (PYso→PYdr, also called PY→PY), from PYso to IN (PY→IN), from TC to TRN (TC→TRN), from TC to PYdr (TC→PY), from TC to IN (TC→IN), from PYso to TRN (PY→TRN), and from PYso to TC (PY→TC). Intracortical AMPA connections (PYso→PYdr and PYso→IN) included synaptic depression. NMDA connections include from PYso to PYdr and from PYso to IN and include synaptic depression. GABA-A connections include from IN to PYso (IN→PY), from IN to neighbor-only IN (IN→IN), from TRN to TC (TRN→TC), and from TRN to TRN (TRN→TRN). GABA-B connections are only from TRN to TC (TC→TRN). Finally, the only connections that are not chemical synapses are the simple compartmental connections between each PYdr compartment and its corresponding PYso compartment. Note

that we use PY→PY to refer exclusively to AMPAergic PYso→PYdr connections.

For all synapses, each source cell is connected to its "nearest-neighbor" ($2 \times$ radius $+ 1$) target cells, where the radius is 10 cells. This makes all connectivity ratios, or how many connections are projecting from each source cell, ~1:20. For our intrathalamic connectivity, since our population sizes are 20, this effectively makes all thalamic connections all-to-all connected, just like in Refs. 10 and 14. For our intracortical connectivity ratio of 1:20, we based this primarily on the model from which we drew our slow-wave oscillation (SWO) mechanism (11) (1:20 with a standard deviation of 5) and subsequent work (12). Other models utilized either higher (ranging from 1:5 to 1:50, with most at 1:10 or 1:20) (31, 32) or lower (1:10) (33) connectivity ratios. Since the original model used a connectivity ratio that was comparable to similar models, and so as not to disturb network dependencies of the SWO mechanism, we elected to use their same intracortical connectivity ratio. Similarly, for the thalamocortical connectivity ratio of 1:20, we based our parameters on Ref. 33 (TC-to-PY ratio of 1:20). This gives us equal intracortical and thalamocortical connectivity ratios, both 1:20.

All synaptic conductances are normalized across the number of incoming connections of a given synapse type. For PY→PY connections this is straightforward, since the sizes of the source and target cell populations are equal, leading to each PY cell receiving 20 of these connections. The maximal conductance of each of these incoming connections is computed to be 1/20th of the total maximal conductance for this synapse type. For connections where the source and population sizes are not equal, such as TC→PY connections, this is more complex. Each TC cell has 20 projections to the PY population, but since there are 20 TCs this equals 400 total projections to go to 100 PY cells. Ultimately, this results in each PY cell receiving connections from 4 TC synapses, resulting in each synapse being normalized to 1/4th of the total maximum conductance. If the total maximum conductances of PY→PY and TC→PY are equal (see next paragraph), then each connection from a single source TC cell to a single target PY cell will have a larger maximal synaptic conductance than each single PY-to-PY connection, but there will be fewer TC-to-PY connections.

Except for the simulations done for Table 2, the total maximal conductances of our intracortical PY→PY and thalamocortical TC→PY AMPA synapses were kept equal to each other and changed simultaneously. We assumed that the ratio between these two maximal synaptic conductances could be held to be equal because of prior thalamocortical models using the same (14) or similar (33) (0.020:0.024) ratios. Additionally, by using equal values for these conductances, we could model the effects of propofol decreasing acetylcholine (ACh) on each of these synapse types in identical ways (see Table 1). We could then compare the effects on the system of treating these conductances heterogeneously (see Table 2) to understand their relative contribution to the case where they are set identically.

The total maximal conductances used for the PY→PY and TC→PY AMPA synapses ranged from 0.002 mS/cm^2 to 0.012 mS/cm^2. These values change in response to the concentration of ACh present, but the relationship between concentration and proportion of change in conductance is not clear, so we were required to explore a range of values; for the relationship of ACh to these conductances, see *Propofol Effects*. We initially based our intracortical and thalamocortical total maximal conductances on the default value used for PY→PY AMPA total maximal conductance in the original cortical SWO model paper (11), 5.4 nS, which is divided over a pyramidal dendritic surface area of 0.035 mm^2 to give 0.0154 mS/cm^2. Since this value is meant to correspond to a non-rapid eye movement (NREM) sleep state that already exhibits low ACh concentration (11), we could use this value to simulate anesthetized states but would need to decrease the value to simulate states of lower levels of anesthesia (see *Propofol Effects*). We did simulate higher values such as 0.0154 mS/cm^2 as in the original paper, but these were not significantly different than the I-state shown in the article and continued the trend shown in the tables of a dominance of I-state.

Model Inputs

For all simulations, to model background activity, excitatory Poisson spike trains were input into all PY, TC, and TRN cells. These spike trains had a firing rate of 40 Hz and were convolved with an exponential with a decay time of 2 ms. The total maximal conductances of these virtual synapses were always held equal to the total maximal conductances of PY→PY and TC→PY AMPA synapses, except for the simulations in Table 2, where the Poisson inputs had conductances of 0.004 mS/cm^2. See the mechanism code (20) for implementation details.

For Figs. 4 and 5, the "synchronizing input" was applied to all PYdr compartments for a duration of 100 ms in each simulation and had a constant amplitude of 1.0 μA/cm^2. For the "desynchronizing input" the input had a duration of 100 ms, but each PYdr compartment received a different constant amplitude randomly pulled from a uniform distribution of −1.0 to +1.0 μA/cm^2. In both cases, the amplitudes did not change for the duration of the stimulus and were 0 outside of the stimulus time.

Propofol Effects

Similarly to our previous work (10), we model how increasing propofol affects the thalamus by changing three parameters: decreasing TC cell H-current maximal conductance ($\bar{g}_H$) and potentiating all $GABA_A$ synapses via increasing maximal conductance ($\bar{g}_{GABA_A}$) and $GABA_A$ decay time constant (τ_{GABA_A}). Propofol may decrease $\bar{g}_H$ (34, 35), although the magnitude of this change is experimentally unknown (36). To shift from a wakelike state to a propofol-anesthetized state, we decrease $\bar{g}_H$ from 0.04 to 0.005 mS/cm^2, which is in line with previous anesthetic and sleep research using this thalamic model (10, 13, 14, 21).

For our propofol simulations, we tripled $\bar{g}_{GABA_A}$ and τ_{GABA_A} for all $GABA_A$ synapses (both cortical and thalamic), since doubling these $GABA_A$ parameters produced only I-state but tripling led to the presence of C-state. We originally based the magnitude of our propofol $GABA_A$ changes on prior modeling work (37). In our previous paper (10), we found that our thalamus-only network could produce persistent alpha oscillations if we doubled or tripled these $GABA_A$ parameters. In Fig. 4 of Ref. 10, we showed that thalamic persistent alpha occurred across a broader range of inputs when

tripling the parameters compared to doubling. In the present article, for all anesthetic simulation variations, doubling $GABA_A$ parameters produces little simulation time with persistent thalamic alpha oscillations. Instead, only by tripling $GABA_A$ parameters do the simulations produce C-state for a substantial amount or majority of simulation time. This may be due to effects on lower-dose behavior caused by additional cortical cell types that we did not include, namely from those of Ref. 37.

Propofol decreases cortical acetylcholine (ACh) (see INTRODUCTION), and we model these cholinergic changes via increasing intracortical AMPAergic synaptic conductances ($\bar{g}_{AMPA:PY\rightarrow PY}$) (11, 12, 33), TC→PY thalamocortical AMPAergic synaptic conductances ($\bar{g}_{AMPA:TC\rightarrow PY}$) (38, 39), and K(Na)-current maximal conductance [$\bar{g}_{K(Na)}$] (11, 12). ACh affects thalamocortical afferent synapses in different ways: decreased nicotinic ACh receptor activation weakens thalamocortical synapses, but decreased muscarinic ACh receptor activation strengthens them (38–43). Based on the rapid desensitization of nicotinic ACh receptors (44), the slowly changing, metabotropic nature of muscarinic receptors, and their similar shifts in natural sleep (45), we believe that muscarinic receptors could exert a stronger effect than nicotinic receptors on thalamocortical afferents, therefore increasing $\bar{g}_{AMPA:TC\rightarrow PY}$ with increasing propofol dose.

The actual proportion of change that ACh can cause in the intracortical and thalamocortical synapses is unclear. Different computational models use a range of proportional increases to $\bar{g}_{AMPA:PY\rightarrow PY}$ caused by ACh, including up to +75% (46) or +15% to +100% (33). Data on how much ACh may increase $\bar{g}_{AMPA:TC\rightarrow PY}$ are much more scarce, but the increase may be as high as +300% (see Fig. 8F of Ref. 39). We therefore focused our synaptic changes on a wide range of decreases from 0.0154 mS/cm^2, the derived value of the low-ACh sleep state used in the cortical SWO model of Ref. 11.

For the K(Na)-current maximal conductance $\bar{g}_{K(Na)}$, we only used two values: 0.10 mS/cm^2 in our wakelike simulation [similar to the tonic, wakelike state of Fig. 14 of the original paper (11)] or 1.33 mS/cm^2 for all anesthetic states. We specifically chose to not make small changes to $\bar{g}_{K(Na)}$ between anesthetic states because it has impacts on the frequency of the SWO produced, which the original paper investigates. Keeping the SWO frequency stable allowed us to more effectively investigate how PAC can arise and how it can be changed by covariation of intracortical and thalamocortical synaptic strength.

Specific Simulation Parameters

The changes to parameters for the wakelike simulation from those of Supplemental Data S2 are as follows (all units in mS/cm^2): $\bar{g}_{AMPA:TC\rightarrow PY}$, $\bar{g}_{AMPA:PY\rightarrow PY}$, and all Poisson inputs set to 0.004, PY $\bar{g}_{K(Na)}$ 0.10, TC $\bar{g}_H$ 0.4, TC $\bar{g}_{K\text{-}Leak}$ 0.001. Additionally for the wakelike simulation, the following synapses were decreased by 60% compared with their values in Supplemental Data S2: $\bar{g}_{NMDA:PY\rightarrow PY}$, $\bar{g}_{NMDA:PY\rightarrow IN}$, $\bar{g}_{AMPA:PY\rightarrow IN}$, $\bar{g}_{AMPA:TC\rightarrow IN}$, $\bar{g}_{AMPA:PY\rightarrow TC}$, and $\bar{g}_{AMPA:PY\rightarrow TRN}$. Our wakelike simulation was the only simulation where we included changes to the six synapse types in the previous sentence; this was done to better align with the wakelike simulations in Figs. 14 and 15 of the original paper (11). The script used to run the wakelike simulation is available with the rest of the simulation scripts (19).

For anesthetic states, all parameters were as given in Supplemental Data S2 unless otherwise indicated, such as changes to $\bar{g}_{AMPA:PY\rightarrow PY}$ and $\bar{g}_{AMPA:TC\rightarrow PY}$ for Tables 1 and 2 and Fig. 6. All parameters are available in the mechanism (20) and simulation (19) code.

EEG Model

We define our simulated EEG as the sum of dendritic voltages of PY cells, as these are considered to be the main contributors (47), band-pass filtered between 0.1 and 50 Hz. The results are unchanged if we considered PY somatic voltages.

Simulations and Reproducibility

All of the simulation parameters (19) and model mechanism code (20) needed to reproduce the simulations shown in this work are available online on GitHub. All simulations were run with the "dev" branch of the MATLAB simulation toolbox DynaSim (48) located online. Individual simulations should be reproducible on a modern desktop computer with access to RAM of 32 gigabytes or higher.

Raw data for Tables 1 and 2 and the bar charts in Figs. 4 and 5 were obtained by visual inspection from simulations that are reproducible from the simulation code (19). The aggregate simulation data are available in Supplemental Data S1.

Human Data

Human experimental data used in Fig. 1 are from a single subject used in Refs. 3 and 4. Analyses in Fig. 1*A* follow those in Refs. 3 and 4. EEG traces were band-pass filtered to 0.1–1 Hz, 8–12 Hz, and 8–20 Hz with a Butterworth filter of order 2. The EEG spectrogram in Fig. 1*B* (not previously published) was computed with the multitapered method (49).

RESULTS

Model of Propofol Acts on Cortical, Thalamic, and Brain Stem Biophysics

We develop a model consisting of interacting thalamic and cortical circuits (see METHODS). Our goal is to understand, and relate to loss of consciousness, the physiological and network mechanisms related to EEG changes as propofol dose increases (3, 4, 7, 50, 51) (Fig. 1). Among the spectral features that we investigate with our modeling are *1*) increased colocalization of the alpha with the peak of slow as dose is increased (Fig. 1*A*), *2*) increased amplitude of the slow oscillation with increasing propofol dose (Fig. 1*A*), *3*) increased low-beta power near loss of consciousness (LOC) and return of consciousness (ROC) (Fig. 1, *A* and *B*), and *4*) decreased mean frequency of alpha and decreased alpha power with higher doses (Fig. 1*B*). We show below that each of these features reflects properties of the model suggestive of mechanisms of loss of consciousness.

We model the cortical circuit using 100 pyramidal cells (PYs) and 20 cortical interneurons (INs) from Refs. 11 and 12 (Fig. 2*A*). The pyramidal cells are modeled with two compartments: the soma (PYso) and the dendrite (PYdr). The

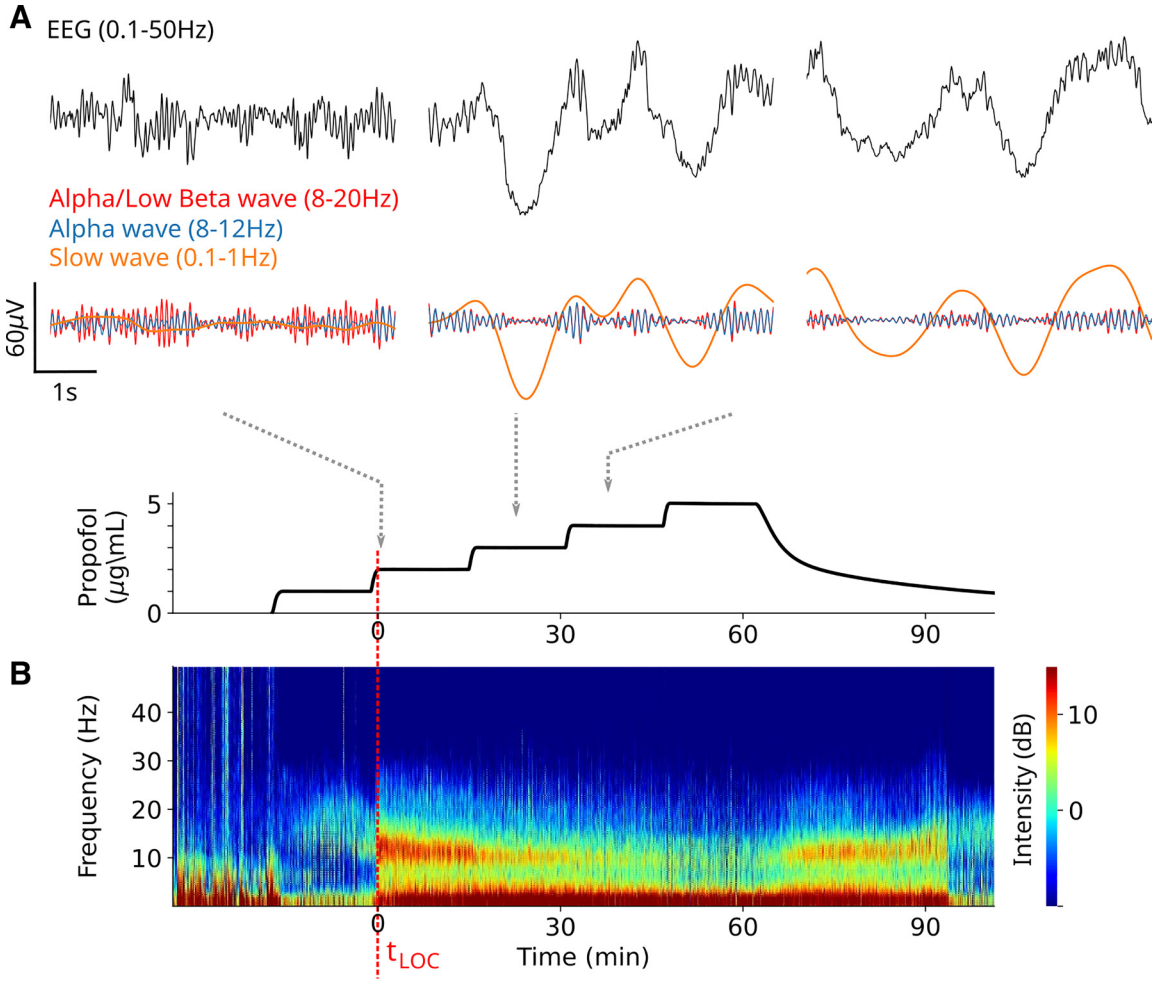

Figure 1. Typical spectral changes seen in the EEG as propofol dose is increased. Human experimental data from a single subject used in Refs. 3 and 4 (see METHODS). *A*: raw EEG traces (*top*) and EEG filtered at alpha/low-beta, alpha, and slow (*middle*) at 3 different doses of propofol (*bottom*) starting near loss of consciousness (LOC) and up to but not including the state of "burst suppression" (9, 52). Low-beta power appears predominantly near LOC. *B*: spectrogram of the EEG during stepped increases in propofol dose in a healthy volunteer.

thalamic circuit is modeled as in Ref. 10, except with 20 thalamocortical cells (TCs) and 20 thalamic reticular neurons (TRNs). Our model currents are conductance based with Hodgkin–Huxley dynamics. Details of the currents used in each neuron type, network connectivity, and all other aspects of the model can be found in METHODS and Supplemental Data S2.

We modeled the addition of propofol as five changes from wakelike conditions (see *Propofol Effects* for further rationales). The first is an increase in the maximal conductance and the inhibition time constant of the GABA receptors, which are known to be produced by propofol (14, 37). The second is a decrease in the maximal conductance of the TC cell H-current (34). Both were used in our previous work without feedback connections from thalamus to cortex (10). The last three effects of propofol account for its action on brain stem circuits: specifically, propofol potentiates inhibitory GABAergic circuits in various arousal centers in the brain stem (1), including cholinergic centers. We focus on the enhanced inhibitory effects on brain stem cholinergic circuits (but see DISCUSSION for other types of neuromodulation). We do not model the brain stem circuitry directly but rather model the effect of decreasing cortical cholinergic tone in the presence of propofol (53–57). This brain stem effect on decreased cortical cholinergic tone is modeled by strengthening *1*) intracortical AMPAergic synaptic conductance, *2*) TC→PY thalamocortical AMPAergic synaptic conductances, and *3*) PY K(Na)-current maximal conductance (see METHODS). As propofol dose is increased, we increase the strength of the intracortical and thalamocortical AMPA conductances. All other propofol changes are not further changed with dose. The EEG of the model is produced by the summation of the voltages in the dendrites of all cortical pyramidal cells (see METHODS).

Propofol Generates Slow Waves in Model Cortex and Alpha/Low-Beta Waves in Model Thalamus

The "wakelike" condition without propofol produces a "depolarized relay state" (21) in thalamus as shown in Fig. 2*B*. In the depolarized relay state, the thalamus can transmit incoming signals; however, no such signals are included in the wakelike state, and thus thalamus is silent (see Refs. 14, 33 for similar models of wakelike thalamus). This simulation shows infraslow oscillations in cortical cells (Fig. 2*B*), which are known to be present in the awake state (58). The slow

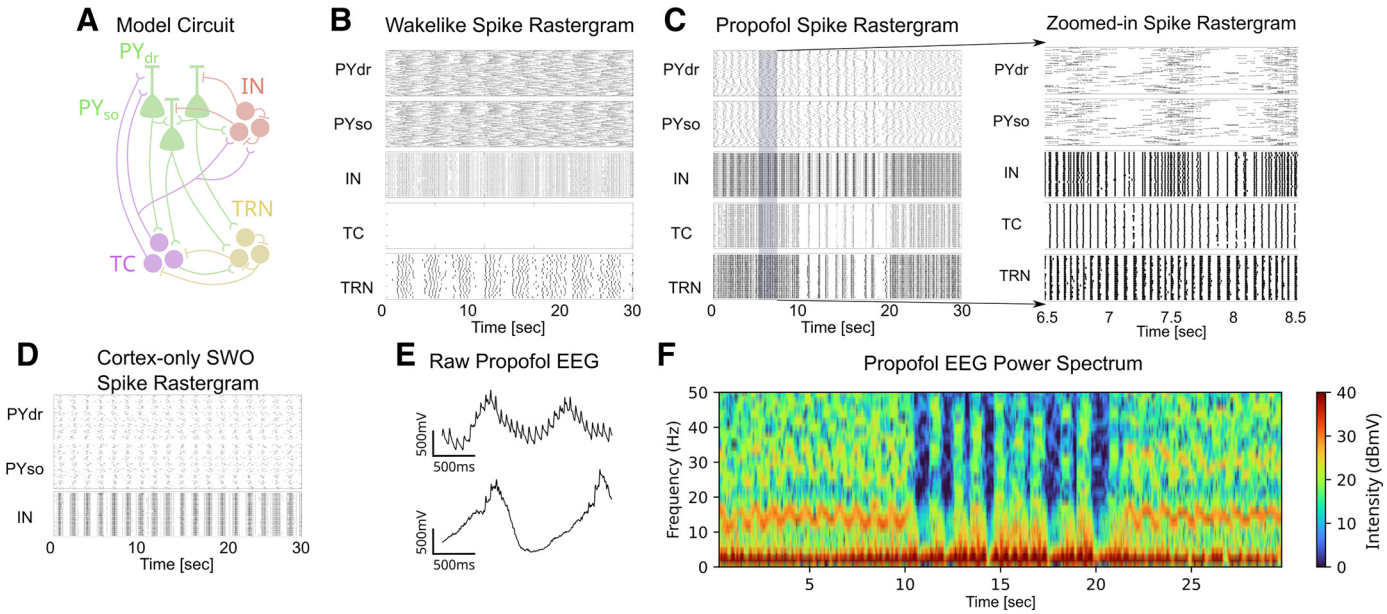

Figure 2. Propofol enables thalamocortical network slow and alpha oscillations. *A*: schematic of thalamocortical network model. IN, cortical interneurons; PY, pyramidal cells (PYdr, dendrite; PYso, soma); TC, thalamocortical cells; TRN, thalamic reticular cells. EEG is modeled as the sum of PYdr voltages. *B*: rastergram of each cell/compartment in wakelike mode with no sensory input, in which each black line represents a spike by each cell/compartment. *C*: rastergram of a simulation under propofol conditions. *Left*: simulation over 30 s. *Right*: a zoom-in showing alpha/low-beta spiking in thalamus. *D*: rastergram of a cortex-only simulation showing slow wave generation in the absence of thalamus when the maximal conductance of the K(Na) current was 0.10 mS/cm^2, representing the level seen during sleep. SWO, slow-wave oscillation. *E*: variations in model EEG. *Top*: EEG taken from 23 to 25 s. *Bottom*: EEG taken from 11 to 13 s. *F*: spectrogram of the model EEG from the simulation shown in *C*.

oscillation in our model originates from the cortex due to the K(Na) current (11) (see METHODS). The firing rates of cells are consistent with known data (59).

With propofol, the thalamocortical network produces prominent slow and alpha/low-beta oscillations that are visible in the raster plots (Fig. 2*C*, *left*). Here we show with a blow-up of the raster plots (Fig. 2*C*, *right*) that the alpha/low-beta oscillation is visible in the thalamic TC cell spiking. The network dynamics can change in time in a way that is examined in detail below. We find that the model cortex alone can generate slow oscillations and thus thalamic involvement is not needed (Fig. 2*D*). With propofol, an alpha oscillation arises in thalamus from the potentiation of GABA-A and the decrease in H-current, as shown in our previous work, which simulates thalamus in the absence of cortex. A description of the alpha-generating mechanism is in Ref. 10 in the section entitled "Propofol induces sustained alpha via changing the balance of excitation/inhibition." This alpha uses the interaction between TC and TRN and engages thalamic spindling mechanisms. In our previous work, we did not include thalamocortical feedback; the present work shows that the thalamic alpha oscillations persist in the presence of thalamic feedback (Fig. 2*C*).

Our model EEG shows strong slow and alpha/low-beta oscillations (Fig. 2*E*). The alpha/low-beta oscillations are more evident (Fig. 2*E*, *top*) in the first and last 10 s of the simulation in Fig. 2*C* than during the middle 10 s (Fig. 2*E*, *bottom*). A spectrogram of the model EEG from the simulation in Fig. 2*C* shows a continuous slow oscillation and a prominent higher-frequency oscillation that switches between alpha/low-beta (8–20 Hz) and a lower average frequency alpha (~ 8 Hz) (Fig. 2*F*).

Propofol Induces Rapid Switching between Two Distinct Thalamocortical Network States

With propofol, the network switches between two mutually exclusive network states on a rapid timescale (seconds) on both the single-cell level and the population level (Fig. 2*C*, Fig. 3, *A*–*F*), each of which can span over multiple cycles of the slow oscillation. The main difference between these states is the periodic cessation of spiking in the thalamus in one state but not the other; when this happens, the cortex and thalamus are simultaneously silent (Fig. 3, *A* and *D*). The thalamic silence occurs because the thalamus enters a silent depolarized state, which stops the thalamus from spiking and thus thalamic input to cortex is lost. We call this network state the "I-state" (short for "interrupt"). In contrast, in the other network state there are no thalamic silent periods because spiking from thalamus is continuous. Thus, we refer to this network state as the "C-state" (short for "continuous").

Both states show slow oscillations and either alpha or alpha/low-beta oscillations in their spiking patterns (Fig. 3, *D*–*F*) as well as in the model EEG (Fig. 3, *G*–*I*) (see METHODS for definition of model EEG). Although the alpha and low-beta rhythms are not a cortically generated rhythm, they appear in the model EEG because of the TC connections onto the pyramidal cell dendrites (Fig. 2*A*). During the I-state the thalamic fast frequency is predominately alpha (8–12 Hz) (Fig. 3, *D* and *G*); during the C-state the fast thalamic frequencies range from 8 to 20 Hz and thus span the alpha/low-beta range (Fig. 3, *F* and *I*). These two network states correspond to different interactions between the slow and the alpha or alpha/low-beta in the EEG. In the I-state, there is

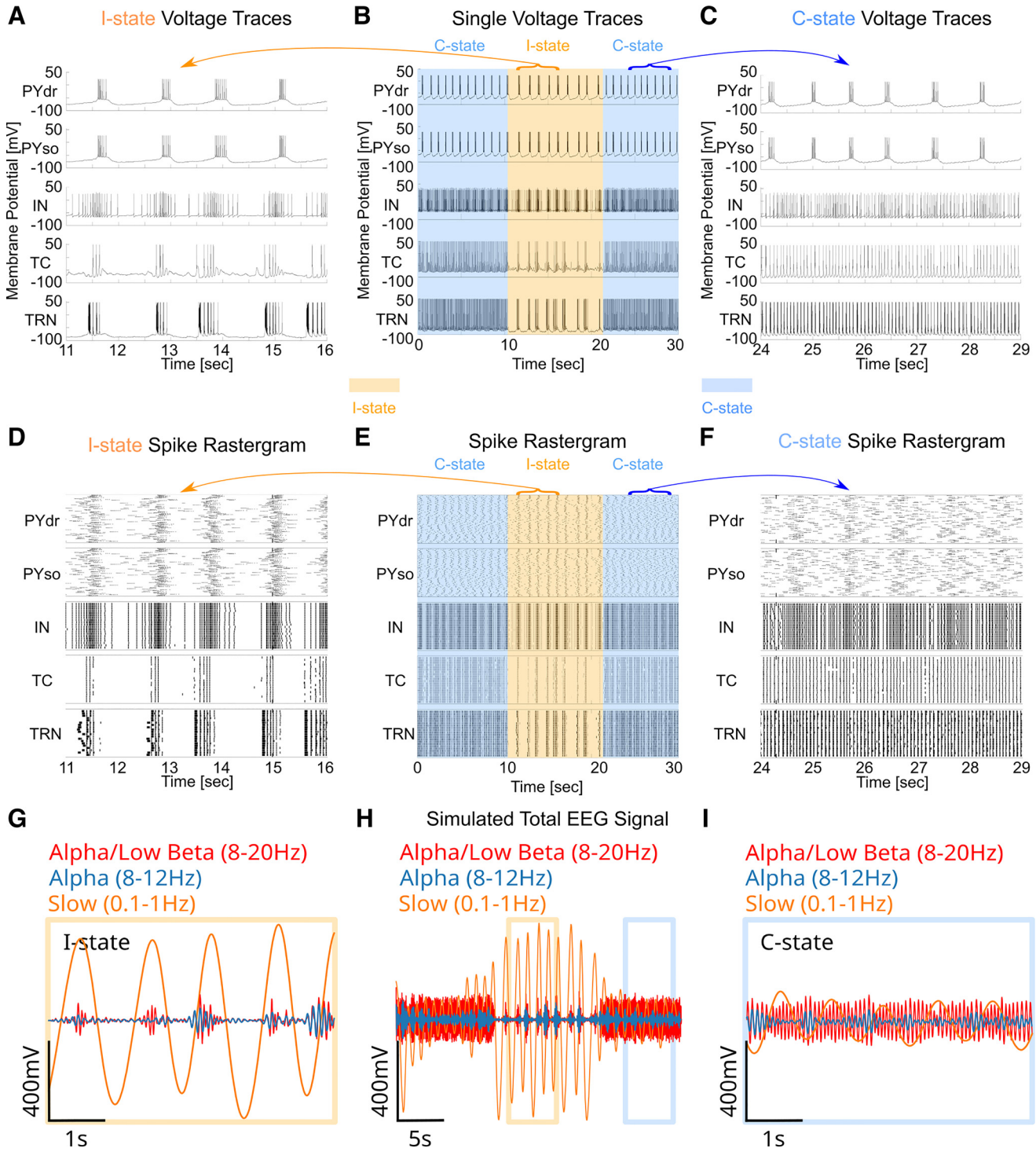

Figure 3. Different slow cycles display I-state or C-state during propofol. *A–C*: representative voltage traces of each cell/compartment during an I-state (*A*), across the entire propofol simulation, with I-state highlighted in orange and C-state highlighted in blue (*B*), and during a C-state (*C*). IN, cortical interneurons; PY, pyramidal cells (PYdr, dendrite; PYso, soma); TC, thalamocortical cells; TRN, thalamic reticular cells. *D–F*: rastergram of all spiking activity during the I-state (*D*), across the entire simulation, with coupling regimes highlighted (*E*), and during the C-state (*F*). *G–I*: model EEG filtered at alpha/low-beta, alpha, and slow during the I-state (*G*), across the entire simulation (*H*), and during the C-state (*I*).

always high-amplitude alpha associated with the peak (or rising phase) of the slow oscillations (Fig. 3*G*); the trough of the slow oscillations corresponds to the simultaneous silent periods in thalamus and cortex (Fig. 3*G*). In contrast, the C-state has a variable relationship between alpha/low-beta and slow (Fig. 3*I*). The thalamic spiking persists continuously throughout the slow oscillation cycles with some variation in the relationship of the alpha/low-beta amplitude to the phase of the slow. In particular, the alpha and low-beta tend to couple at different phases of the slow oscillation during

the C-state. Our simulations suggest that one possible coupling during the C-state is a transient coupling of alpha to the trough of the slow oscillation as seen on some slow cycles in Fig. 3*I*, as well as in experimental literature (3, 4). When this occurs, the low-beta couples to a different phase of the slow oscillation (Fig. 3*I*). Note that in the C-state the slow oscillation has lower amplitude than in the I-state (compare Fig. 3*G* and Fig. 3*I*).

In summary, the thalamocortical network rapidly switches between two states with propofol. The I-state is characterized by periods of coordinated thalamic and cortical silence as well as high cortical synchrony. In contrast, the C-state displays ongoing activity in thalamus and less cortical synchronization. The EEG during the I-state shows alpha oscillations but lacks low-beta oscillations, large-amplitude slow oscillations, and colocalization of the alpha with the peak of the slow. In contrast, during the C-state the EEG has alpha and low-beta oscillations, smaller-amplitude slow oscillations, and variable alpha-slow coupling, with alpha coupling to the trough being one possibility.

Cortical Synchrony Determines Thalamocortical State by Modulating Network Feedback Dynamics

Cortical synchrony is a critical determinant of thalamocortical state under propofol, determining both the thalamic state (continuous spiking or interrupted spiking) as well as the spectral features of each state. The spiking in the cortex is noticeably more synchronized during the I-state than in the C-state (Fig. 3, *D* and *F*). The level of cortical synchrony affects the depolarization level of the thalamus and thus the thalamic spiking dynamics. Indeed, the less synchronized cortex in the C-state allows the thalamus to remain hyperpolarized and thus to continue engaging spindle dynamics (10), whereas the additional synchronization in cortex during the I-state depolarizes the thalamus into its silent depolarized state. Thus, cortical synchrony is a critical determinant of thalamocortical state under propofol.

The C-state and I-state have different types of thalamocortical interactions under propofol. In the C-state, when the thalamus is spiking continuously (because of low cortical synchrony), the thalamus provides positive feedback to the cortex. In the I-state, the synchronous cortical input stops the thalamus by putting it in its silent depolarized phase, whereas cortical silence promotes thalamic spiking (because of the hyperpolarization of the thalamus). Thus, the type of feedback in the I-state is homeostatic: cortical excitation leads to negative feedback from thalamus via silencing thalamus, whereas reduced cortical firing causes excitatory feedback from thalamus. The switch in feedback regimes (and thus network state) is abrupt because, as soon as the cortical synchronization level is sufficient to silence the thalamus, the network switches to homeostatic feedback.

The type of corticothalamic feedback dictates the spectral coupling observed during the different states. In the C-state, the alpha often occurs near the trough of the slow wave, whereas the low-beta occurs more toward the peak of the slow wave. This phenomenon stems from the influence of cortical spiking on the excitation level of the thalamus: when cortical spiking is low, as in the trough of the slow wave, the thalamus is more hyperpolarized and thus has a lower frequency of spiking (alpha spiking). In contrast, when the cortical spiking is higher, as in the peak of the slow wave, the thalamus is more depolarized and thus the thalamic spiking is at beta. The positive feedback from thalamus to cortex engages the activity-dependent K(Na) current, with the thalamus giving less excitation (alpha) to cortex when the cortical activity is low and more excitation (low-beta) when the cortical excitation is high. Note that this accounts for increasing frequency of the K(Na)-mediated slow oscillations between the wakelike state (~0.2 Hz) and the C-state (1 Hz) (Fig. 2, *B* and *C*). In contrast, when the network is in its homeostatic feedback regime (I-state), cortical synchrony leads to thalamic silence, which in turn leads to a profound loss of cortical spiking. This simultaneous loss of thalamic and cortical spiking is reflected in a large slow wave trough with no alpha coupling. The thalamus responds to the loss of cortical input by hyperpolarizing into its spindling regime and again spiking, now at predominately alpha, which depolarizes the cortex into its active phase. The diminished cortical K(Na), which decreased during the cortical inactive phase, additionally primes the cortex to spike more synchronously in response to the thalamic input. The more synchronous spiking during the cortical active phase is reflected in the EEG as a higher-amplitude peak in the slow wave. The alpha spiking in the thalamus is coupled to the peak of the slow wave since this is the only phase at which the thalamus is active.

Summarizing the connection between cortical synchronization and thalamic state, we find that under propofol the thalamocortical network can abruptly switch between two dynamic network states governed by the level of synchronization in the cortex. The spectral features of the EEG during these two states are the results of a switch in thalamic feedback dynamics: positive feedback during the C-state and homeostatic feedback during the I-state. In particular, we find that during the state of positive corticothalamic feedback (C-state) the amplitude and duration of the slow oscillation are controlled by the kinetics of the activity-dependent K(Na) current in the cortex, whereas during the state of homeostatic corticothalamic feedback (I-state) the amplitude and duration of the slow oscillation are influenced by the thalamic feedback. The larger-amplitude slow waves during the I-state are a consequence of engaging the homeostatic thalamocortical feedback, whereas the low-amplitude slow waves during the C-state result primarily from cortical K(Na) dynamics.

To verify the relationship between the cortical synchronization and the thalamocortical state, we tested whether we could change the thalamocortical state by introducing artificial cortical synchronization or desynchronization. We applied 100 ms of either a synchronizing or desynchronizing input to cortex during a period when the system was in a C-state. Artificial synchronization of cortex switched the thalamocortical network to an I-state, whereas with artificial desynchronization the thalamocortical network remained in the C-state (Fig. 4). These results support cortical synchronization as a driver of C-state-to-I-state transitions. When cortical synchronizing or desynchronizing inputs were applied to the network when the system was in an I-state, we found that desynchronizing

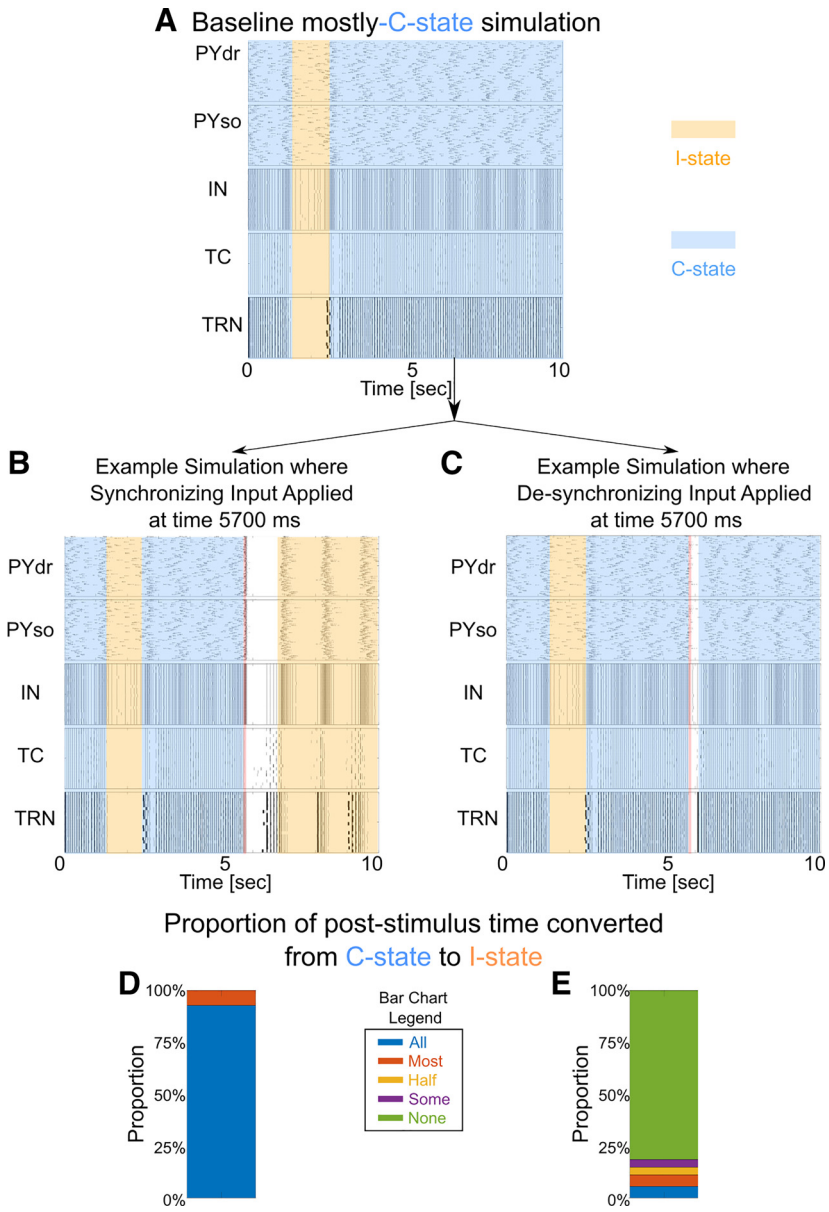

Figure 4. Cortical synchronization induces a C-state-to-I-state transition. *A*: rastergram of a "baseline" simulation in which most of the time is spent in the C-state. IN, cortical interneurons; PY, pyramidal cells (PYdr, dendrite; PYso, soma); TC, thalamocortical cells; TRN, thalamic reticular cells. For every 100-ms interval expressing the C-state in the baseline simulation, two additional simulations were run: one simulation where a synchronizing input stimulus (see METHODS) was applied to PYdrs during that specific 100-ms interval (example shown in *B*) and another simulation where a desynchronizing input stimulus (see METHODS) was applied to PYdrs over that specific 100-ms interval (example is shown in *C*). *B*: rastergram showing an example simulation where synchronizing input was applied during time 5,700–5,800 ms, causing the remainder of the simulation to exhibit I-state behavior. Red line marks the time of the input. *C*: rastergram showing an example of desynchronizing input for the same time interval as *B*, but where the simulation almost completely remains in the C-state. *D*: bar graph showing, for all simulations receiving synchronizing inputs at different times, the proportion of poststimulus simulation time that exhibited a C-to-I-state transition. Scoring was done by visual inspection, where each simulation was marked as "All" if >95% of simulation time after the synchronizing input exhibited I-state; analogously, each simulation was otherwise marked as "Most" (95–50%), "Half" (~50%), "Some" (50–10%), or "None" (<10%). The bar chart is the summation of all simulations receiving a synchronizing input and indicates that the artificial synchrony brought by the synchronizing input was very effective at converting C-states to I-states. *E*: similar to *D* but for baseline simulations receiving desynchronizing input, indicating that desynchronizing input was not effective in eliciting C-state-to-I-state transitions.

inputs induced a transition to the C-state, whereas the network remained in the I-state in response to synchronizing inputs (Fig. 5). These results highlight cortical desynchronization as a key determinant of I-state-to-C-state transitions and thus a key determinant of thalamocortical state under propofol.

Propofol Potentiates TC Feedback via Brain Stem Neuromodulation, Facilitating Synchronization of Cortex and a Switch to the I-State as Dose Increases

In *Cortical Synchrony Determines Thalamocortical State by Modulating Network Feedback Dynamics*, we showed that cortical synchronization is a key driver of C-state-to-I-state transitions in corticothalamic circuits. Here we propose the physiological mechanism by which increased cortical synchronization occurs as propofol dose is increased.

We model increasing propofol dose by progressively decreasing ACh neuromodulation on corticothalamic circuits (see METHODS): we increased maximal AMPA synaptic strength between cortical pyramidal cells ($\bar{g}_{\mathrm{AMPA:PY\rightarrow PY}}$) and from TC cells to cortical pyramidal cells ($\bar{g}_{\mathrm{AMPA:TC\rightarrow PY}}$), which strengthens feedback from thalamus to cortex. As propofol dose is increased in our model, the amount of time spent in the C-state progressively decreases and is replaced by more time spent in the I-state (Table 1). The progression in colocalization of alpha to the peak of the slow oscillation recapitulates the findings in subjects undergoing propofol anesthesia-induced unconsciousness.

To determine whether the change to more I-states relies primarily on TC→PY or PY→PY synapses, we looked at the incidence of I-states when changing one of these synapses at a time. We found that the dose-dependent increased time spent in the I-state is primarily due to increasing the TC→PY AMPA synapse (Table 2). The strengthened feedback leads to more synchronized cortical cells, which in turn causes the switch to the thalamocortical homeostatic feedback regime

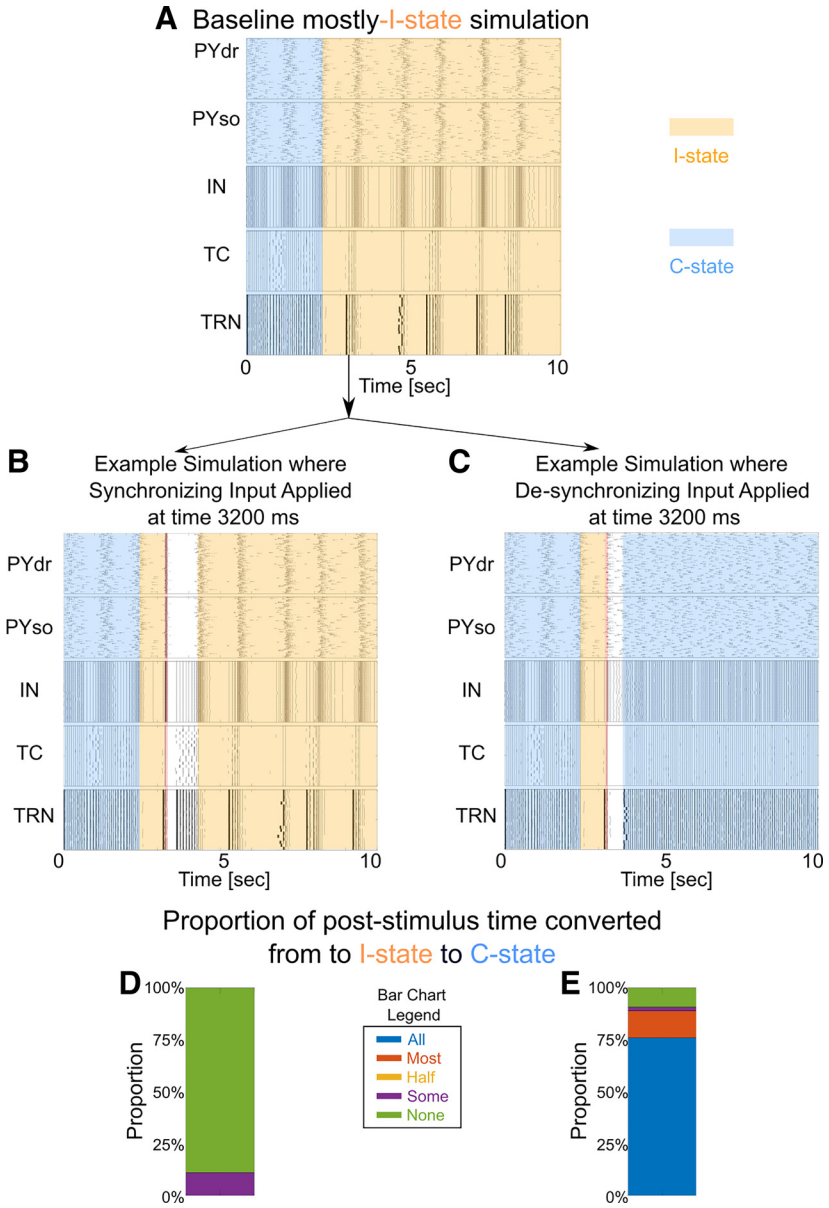

Figure 5. Cortical desynchronization causes an I-state to C-state transition. This figure is analogous to Fig. 4 but studying I-to-C transitions instead of C-to-I transitions. *A*: rastergram of a "baseline" simulation in which most of the time is spent in the I-state. IN, cortical interneurons; PY, pyramidal cells (PYdr, dendrite; PYso, soma); TC, thalamocortical cells; TRN, thalamic reticular cells. For every 100-ms interval expressing the I-state in the baseline simulation, two additional simulations were run: one simulation where a synchronizing input stimulus (see METHODS) was applied to PYdrs over that specific 100-ms interval (example shown in *B*) and another simulation where a desynchronizing input stimulus (see METHODS) was applied to PYdrs over that specific 100-ms interval (example shown in *C*). *B*: rastergram showing an example simulation where synchronizing input was applied during time 3,200–3300 ms but did not lead to C-state behavior. Red line marks the time of the input. *C*: rastergram showing an example of desynchronizing input for the same time interval as *B*, but where the remainder of the simulation exhibits C-state behavior. *D*: bar graph showing, for all simulations receiving synchronizing inputs at different times, the proportion of poststimulus simulation time that exhibited an I-state-to-C-state transition. Scoring was done as in Fig. 4. The bar chart is the summation of all simulations receiving a synchronizing input and indicates that the artificial synchrony brought by the synchronizing input was not effective at converting I-states to C-states. *E*: similar to *D* but for baseline simulations receiving desynchronizing input, indicating that desynchronizing input was very effective in eliciting I-state-to-C-state transitions.

(see *Cortical Synchrony Determines Thalamocortical State by Modulating Network Feedback Dynamics*) associated with I-state dynamics.

That the C-state-to-I-state switch requires thalamocortical feedback is supported by the finding that, in the absence of TC feedback, the thalamocortical networks remain in the C-state (Fig. 6). It also shows that the cortical synchronization caused by the K(Na) production of the slow wave does not produce sufficient cortical synchrony to induce the C-state-to-I-state transition. In contrast, we showed in *Cortical Synchrony Determines Thalamocortical State by Modulating Network Feedback Dynamics* that the switch from the I-state to the C-state is facilitated by cortical desynchronization. This can occur physiologically under propofol because of cortical noise (Fig. 3).

The increasing time spent in the I-state with higher doses of propofol accounts for several dose-related EEG findings including *1*) less low-beta because this frequency is predominantly in the C-state, *2*) more lower-frequency alpha because the alpha in the I-state has a lower average frequency than the alpha in the C-state (see Fig. 4*B*), *3*) decreased alpha power because alpha is only present for a short period on the peak of the slow wave in the I-state, *4*) loss of trough-max because trough-max is seen only in the C-state and only occasionally in that state, *5*) increased peak-max due to thalamic alpha spiking occurring only during the peak of the slow wave in the I-state, and *6*) increased slow-wave amplitude/power due to the I-state having larger-amplitude slow oscillations as a result of increased cortical synchronization and its coordinated corticothalamic silent states.

DISCUSSION

Overview and Clinical Implications

The anesthetic propofol produces oscillatory signatures on the electroencephalogram (EEG): prominent alpha/low-beta oscillations (8–20 Hz), slow oscillations (0.5–2.0 Hz),

Table 1. *Proportion of time spent in the C-state when both TC→PY and PY→PY are set to the corresponding maximal g_{AMPA} under propofol conditions*

g_{AMPA}	Mean ± SD
0.002	83.7 ± 9.81%
0.003	83.26 ± 16.74%
0.004	70.37 ± 25.87%
0.005	44.39 ± 30.94%
0.006	32.03 ± 34.22%
0.007	15.61 ± 23.60%
0.008	6.97 ± 15.61%
0.009	4.15 ± 11.35%
0.01	1.29 ± 3.26%
0.012	0.65 ± 3.27%

The units for AMPAergic synaptic conductance (g_{AMPA}) are mS/cm^2. For each g_{AMPA} value, measurements were taken across ~70 independent simulations that were each 30 s long. Any simulation time not spent in C-state corresponded to time spent in I-state. For comparison, we used $\bar{g}_{AMPA:PY\rightarrow PY}$ and $\bar{g}_{AMPA:TC\rightarrow PY}$ = 0.004 mS/cm^2 in our wakelike simulations (which do not have propofol effects), both synapses equal to 0.005 mS/cm^2 in our propofol simulation used in Fig. 3 and related figures, and both synapses equal to 0.008 mS/cm^2 in our disconnected "high-dose" propofol simulation in Fig. 6. Since the true values of these synaptic conductances under propofol are not known (see *Propofol Effects*), we infer that higher values of these synaptic conductances correspond to higher propofol doses owing to the dramatic reduction of C-state in favor of I-state at high values. PY, pyramidal cell; TC, thalamocortical cell.

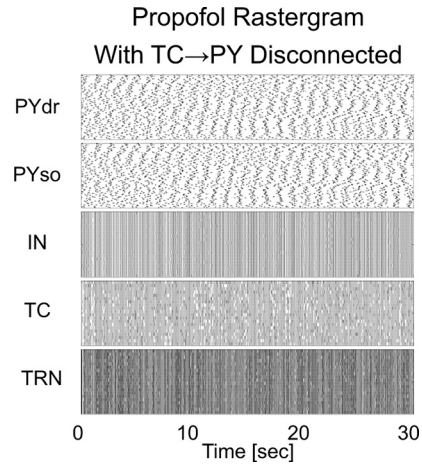

Figure 6. Lack of thalamocortical connections disables transitions from C-state to I-state. Rastergram of a "high-dose" [maximal AMPAergic synaptic conductance ($\bar{g}_{AMPA:PY\rightarrow PY}$) = 0.008 mS/cm^2] propofol simulation where thalamocortical cell (TC)→pyramidal cell (PY) AMPA synapses have been set to 0. Simulations without thalamocortical feedback never exhibited an I-state. IN, cortical interneurons; PYdr, dendrite; PYso, soma; TRN, thalamic reticular cells.

and increased colocalization of the alpha to the peak of the slow with increasing effect site concentration (4). Here we use computational models to examine the role of brain stem, thalamus, and cortex in producing these oscillations and shaping the interactions between them. Specifically, our results help to understand the biophysical origin of the rhythms and the role of the rhythms in producing loss of consciousness.

One surprising finding in our simulations is that the thalamocortical network switches at a timescale of seconds between two dynamic states characterized by continuous alpha/low-beta in thalamus (C-state) or by transient interruption of the thalamic alpha (I-state). In the latter, the alpha is colocalized to the peak of the slow rhythm (peak-max), whereas in the former there need not be consistent colocalization. What is called trough-max in the literature is here a special case of the C-state seen in the literature at sustained low doses of propofol that are used in experiments with volunteers; with clinical use, these stages are passed through quickly (3, 4, 7). In the I-state, cortical and thalamic silent periods are coordinated, which is the reason for the peak-max coupling. We further show that increases in propofol dose lead to statistically more prevalence of the I-state versus the C-state. Cortical synchrony is a key driver of the transitions between the I-state and the C-state: we show that corticothalamic state transitions are mediated by the level of cortical synchrony. We illustrate this by introducing artificial synchrony and desynchrony in cortical spiking during ongoing periods of the I-state or the C-state (Figs. 4 and 5). Cortical synchrony can switch the C-state to the I-state, and desynchrony can cause the I-state to switch to the C-state. One determinant of cortical synchrony in our network is thalamocortical feedback; this is strengthened by neuromodulatory changes related to propofol dose, biasing the expression of the I-state over the C-state as the dose of propofol increases.

Our model reproduces several clinical EEG observations as propofol dose increases: less low-beta power, lower-frequency alpha, less alpha power, loss of trough-max coupling, increased peak-max coupling, and increased slow-wave amplitude/power. The model provides physiological and network mechanisms for these effects, which give insights into how propofol works to produce loss of consciousness. The dynamic switch between two types of thalamocortical feedback, positive feedback in the C-state and homeostatic feedback in the I-state, determines the corticothalamic spiking patterns as well as the EEG spectral changes that correlate with each state. As dose is increased, brain stem effects on the

Table 2. *Proportion of time spent in the C-state with differential values of TC→PY and PY→PY maximal gAMPA conductance*

PY→PY g_{AMPA}, mS/cm^2	TC→PY g_{AMPA}, mS/cm^2			
	0.004	0.006	0.008	0.01
0.004	58.49 ± 25.07%	32.69 ± 30.00%	12.79 ± 14.31%	4.82 ± 11.01%
0.006	54.53 ± 32.70%	21.33 ± 24.49%	8.42 ± 10.33%	3.15 ± 8.92%
0.008	52.52 ± 25.46%	27.92 ± 27.83%	6.05 ± 11.04%	4.67 ± 8.56%
0.01	43.06 ± 25.29%	17.71 ± 19.18%	7.07 ± 13.46%	2.36 ± 5.54%

Values are means ± SD. For each set of AMPAergic synaptic conductance (g_{AMPA}) values, measurements were taken across ~40 independent simulations that were each 30 s long. PY, pyramidal cell; TC, thalamocortical cell.

thalamocortical feedback enable increased cortical synchrony, and thus I-states become more prevalent. The increasing proportion of time spent in the I-state with larger doses of propofol in our model accounts for all the experimental spectral changes mentioned above associated with increasing propofol dose. Cortical synchronization has been found experimentally to relate to the level of unconsciousness (17), and thus these EEG measures may indicate the level of propofol-induced unconsciousness.

Our model helps explain why earlier work emphasized the trough-max state (3, 4): they were filtering in the alpha band (8–12 Hz), whereas our C-state shows nonslow oscillations between 8 and 20 Hz. As can be seen in Figs. 1 and 3*I*, the alpha band is sometimes found in the trough of the slow oscillation, with beta oscillations at other phases. Lower doses of propofol associated with the time of loss of consciousness (LOC) are also characterized by a larger beta power than seen either at resting wakefulness or at higher doses of propofol (3, 4, 6, 7, 60). Our modeling suggests that this beta comes from thalamus in the presence of propofol. The model also suggests why the lower doses of propofol that commonly occur around LOC are associated with a light state of anesthesia (4): the beta oscillations communicated to the cortex are believed to be the basis of long-distance coordination in cortex (61), and hence signals from the thalamus can be transferred more widely throughout the cortex. By contrast, modeling has suggested that alpha disrupts such coordination (62, 63), which is consistent with alpha being the predominant rhythm with deeper levels of propofol anesthesia. Thus, a ratio of low-beta power to alpha power may be a way to monitor the depth of propofol-induced unconsciousness near the onset of LOC.

Relation to Prior Modeling Work

Our previous computational modeling (10) suggested thalamus as the source of propofol-induced alpha (although not low-beta) and showed that dose-dependent coupling between alpha and slow occurred if slow oscillations were imposed on the thalamus from cortex via an "open-loop." In this work, we simulate a "closed-loop" thalamocortical network of Hodgkin–Huxley cells with feedback from both thalamus to cortex and cortex to thalamus. Most of the results we find are a consequence of this feedback. Our cortical model is derived from models that can generate slow oscillations during sleep (11, 12).

Although prior modeling demonstrated that thalamocortical circuits could produce propofol alpha oscillations (13, 14), or propofol alpha and slow (33), our previous work (10) was the first modeling investigation of which we are aware into the unique alpha-slow PAC dynamics of propofol. The essential results of the previous paper continue to hold in our present model: *1*) The alpha is generated by propofol acting on thalamic circuits; *2*) our previous hypothesis that propofol-induced slow oscillations can come from the cortex is supported by the new modeling; and *3*) cortical slow and alpha can interact in different ways depending on the hyperpolarization of the thalamus. However, details of the coupling between alpha and slow oscillation are altered from our previous work by the interaction between the thalamus and cortex, which was not explicitly modeled in that prior work.

Some mechanisms have been changed from our prior model and yield a better fit with experimental data: *1*) in the prior thalamus-only model, the maximal thalamic spiking frequency under propofol was alpha. In this modeling work, the thalamus can spike as high as low-beta (~20 Hz) [which has been seen in experiments (64, 65)]. *2*) In the previous model, thalamic alpha emerged only during the cortical silent phase of the slow during low-dose propofol and only during the cortical active phase of the slow during high dose. In the present model, in which the hyperpolarization level of the thalamus is influenced by the cortex, we find that during the C-state the thalamus does not hyperpolarize enough to completely stop thalamic spiking during the cortical active phase; rather, the thalamus produces alpha/low-beta throughout all phases of the slow oscillation. As a result of this, alpha/low-beta is more prominent, and thus will show higher power, during low-dose time periods, in which the C-state is more prevalent (see Fig. 1*B*) (3, 4, 7). *3*) The addition of thalamocortical feedback allows changes in cortical synchronization with increase in dose: continuous alpha/low-beta in thalamus results from less cortical synchronization, and hence the slow waves that appear in cortical EEG have a significantly lower amplitude and greater variability (Fig. 1, *B* and *C*; Fig. 3, *G* and *I*) during the C-state than during the I-state (4). *4*) Another difference from previous work is that, in the present model during the I-state, the thalamic silence during the cortical silent period is due to depolarization from corticothalamic excitation rather than hyperpolarization as suggested by the thalamus-only model. This difference is significant in linking cortical synchronization to state changes: cortical synchronization depolarizes thalamus out of its alpha spiking into a silent state, changing the dynamics to the I-state. *5*) In this article, we explicitly model the cortex rather than using it just as an input to the thalamus. Thus, we were able to model the EEG by using the sum of pyramidal cell dendritic voltages (47).

Other models of alpha oscillations exist in the literature with cortical as well as thalamic sources. Most of the modeling literature about cortical alpha concerns the awake state (Refs. 63, 66–70, but also see Ref. 13). In the context of propofol anesthesia, however, the prominent alpha observed in the EEG is likely to come from the thalamus: alpha oscillations under propofol are globally coherent, whereas slow oscillations are not (2, 3). This suggests that cortical alpha is coming from a noncortical source such as the thalamus. Our earlier modeling suggests that the thalamus can produce an ongoing alpha in the presence of propofol via potentiated GABA-A employment of thalamic spindle mechanisms (10). This is a prediction of both our previous and present model that remains to be tested experimentally. A recent experimental and computational study looking at oscillations with another GABAergic anesthetic, isoflurane, suggests that this anesthetic can also generate thalamic alpha oscillations (71).

Propofol, Slow Oscillations, and Brain Stem-Mediated Neuromodulation

A notable interpretation of this model is that the anesthetic effects of propofol depend on neuromodulatory effects as much as on GABA-A inhibition and TC cell H-current. ACh release in rodent frontal cortex can be decreased by 70–85% in the presence of propofol (53, 54). In the model,

lowered ACh affects several cortical currents: *1*) lowered ACh increases the K(Na) current (45, 72), enabling slow oscillations; *2*) lowered cortical ACh increases intracortical AMPAergic synaptic conductances (11, 12, 33); and *3*) cortical muscarinic receptors respond to lowered ACh by increasing thalamocortical AMPA conductance (38, 39). The latter is critical in our model for producing the greater synchrony of the cortex needed to switch to the I-state more often as dose is increased.

Noradrenergic tone is also decreased in the presence of GABAergic anesthetics: propofol and sevoflurane potentiate inhibitory GABAergic synaptic activity from the preoptic area of the hypothalamus onto noradrenergic neurons of the locus coeruleus, which diffusely project to cortex among other areas (73). In the cortex, norepinephrine (NE), as well as ACh, abolish slow oscillatory activity mediated by cortical UP and DOWN states (39). Thus, lowered cortical NE due to propofol may work collaboratively with ACh in producing increased slow oscillations in cortex. Unlike ACh, which nonspecifically suppresses PY→PY and TC→PY excitatory (AMPA), NE selectively suppresses intracortical excitatory inputs (39). Although we find that the dominant effect on cortical synchronization with propofol is due to increasing thalamocortical AMPA conductance, NE likely contributes to the overall cortical synchronization by increasing the intracortical AMPA conductance.

We note that propofol likely also utilizes known slow mechanisms via its effects on noncholinergic brain stem neuromodulatory systems. Propofol not only affects the cholinergic sources in the basal forebrain, laterodorsal tegmental area, and pedunculopontine tegmental area but also inhibits the tuberomammillary nucleus, locus coeruleus, dorsal raphe nucleus, ventral periaqueductal gray, and lateral hypothalamus (1, 9). These areas respectively provide histamine, norepinephrine, serotonin, dopamine, and orexin/hypocretin to the cortex (1, 9). Many of these neuromodulators affect various potassium currents that are critical in known models of slow oscillations, including the K(Na) current, the persistent sodium (NaP) current, and potassium leak currents (45, 72). These neuromodulators can also affect both excitatory and inhibitory currents in the cortex and can change the relative impact of thalamocortical synapses (39, 45, 74). Additionally, cortical neuromodulation by NE, as well as ACh, is known abolish SWO and is active during awake/relay states (18). There is still much we do not understand about how all these neuromodulators work in concert together (18, 33).

It is known that the cholinesterase inhibitor physostigmine reverses propofol LOC (55); assuming LOC depends on slow oscillations and synchronization of the cortex, our model suggests that the engagement of ACh-modulated currents by propofol may explain this experimental result: physostigmine acts to increase ACh levels, which would decrease $\bar{g}_{K(Na)}$ in our model and stop the K(Na)-dependent slow oscillation produced by propofol. ACh also acts to weaken thalamocortical connections (39) and therefore release the cortex from oversynchronization; less synchronized states are associated with the awake state. Thus, loss of ACh may be a major contributor to propofol-induced loss of consciousness. The fact that our model requires neuromodulatory changes to produce propofol oscillations and their coupling suggests that the effects of propofol on the brain stem may be critical for its oscillatory phenomena, which is supported by active experimental research on propofol and other anesthetics (18, 56, 75–78). Since the transition from C-state to I-state in our model is associated with lowering ACh (without changing GABAergic effects), we predict that a smaller dose of physostigmine may produce less I-state and more C-state and thus may lead to more EEG low-beta, higher-frequency alpha, increased alpha power, less peak-max, and lower slow-wave amplitude.

Propofol, Slow Oscillations, and Sleep

Our work suggests that propofol utilizes not only thalamic spindling mechanisms (10) but also natural sleep slow mechanisms and changes in neuromodulation to produce its oscillatory effects. The K(Na) current is the primary mechanism of slow oscillation generation in the cortical sleep slow oscillation model we used (11, 72, 79). Most other slow oscillation models rely on a combination of changes to cortical excitatory/inhibitory plasticity and/or the persistent sodium (NaP) current (23–25, 27, 29, 33). The NaP current has been shown to be functionally coupled to the K(Na) current (80), and therefore the K(Na) current may contribute to these mechanisms. Some models of slow UP state initiation, also called DOWN-to-UP transitions, rely on random cortical excitation (24), synaptic plasticity changes (23, 33), or TC initiation of cortical slow UP states (29). In our simulations, the DOWN-to-UP transition is not reliant on the above mechanisms but rather initiates when the hyperpolarizing K(Na) current in a PY cell has decayed sufficiently to allow significant PY spiking. In our I-state, however, the slow oscillation is primarily a manifestation of the change in thalamocortical feedback dynamics. The network feedback switches from a positive feedback dynamic in the C-state to a homeostatic feedback dynamic in the I-state. The homeostatic feedback produces wide swings in the amplitude of the slow oscillations, which differs from low-amplitude K(Na)-mediated slow oscillation in the C-state. Future work designed to differentiate natural sleep slow oscillations versus general anesthetic slow mechanisms will enable finer-grained experiments into how the loss of consciousness occurs in these two distinct states.

Propofol, Memory Consolidation, and Aging

Our investigation of thalamocortical dynamics under propofol may have implications for memory and aging. During natural sleep, memory consolidation onto cortical axo-dendrite connections likely occurs during the nesting of hippocampal ripples during thalamic spindles, which themselves are nested inside thalamocortical sleep slow oscillations (81). Based on our present and previous work (10), propofol alpha and slow oscillations employ some of the same mechanisms used during sleep-related memory consolidation: propofol alpha derives from the thalamic spindling mechanism, and propofol slow oscillations engage the cortical K(Na) current also engaged by sleep. Proper memory consolidation requires correct encoding of worthwhile memories during sleep (82), but if application of propofol abnormally activates some of the same oscillations in this process, this may lead to invalid memory consolidation or interfere with synaptic-dendrite networks involved in storing memory. A recent experiment showed promising results in using propofol to

disrupt reconsolidation of traumatic memories (83), which could help treat posttraumatic stress disorder patients. Additionally, alpha power and, to a lesser extent, slow power under propofol may indicate a subject's "brain age" (84). Our modeling predicts that propofol alpha may predominantly arise from the thalamus, and therefore a decrease in propofol alpha power across age could correlate with brain fitness via losses in the ability of the thalamus to burst at alpha or enter the spindling regime (84), myelination retention of thalamocortical afferents (85), or the strength of thalamocortical synapses onto cortical dendrites (86).

Caveats, Limitations, and Future Modeling

Our model is relatively small considering its significant complexity: there are a total of 160 neurons among multiple types in both cortex and thalamus. Larger models may sometimes display behavior that is not captured in smaller ones because of the degree of heterogeneity that is possible. Delineating such behavior is beyond the scope of this work. Also, not included in our model is complexity associated with the multiple layers of the cortex and the multiple kinds of nuclei in the thalamus. The use of Hodgkin–Huxley modeling in this study is justified when examining the effects of anesthetic drugs such as propofol, which work to change the kinetics of synaptic receptors and the conductances of intrinsic membrane currents that interact to sculpt the network behavior (1). As such, the size and complexity of the model is driven by the questions asked. We found that simpler models, both in cellular components and neuron numbers, were not sufficient to replicate the spectrum of propofol-induced EEG changes explored in this article and understand their mechanisms. As to further detail, our philosophy is to look for a minimal model, however complex, that will reproduce the interactions of the slow and alpha rhythms consistent with experimental results. Regarding the effects of brain stem modulation, we focused almost entirely on cholinergic modulation. Effects of other neuromodulators, briefly mentioned, are left for future work. Even the effects of ACh were not completely investigated; notably, we did not look at the effects of changing K(Na) strength with successively larger effect site concentrations of propofol.

Heterogeneity in TC→PY and PY→PY strength and connectivity across cortical regions and layers may contribute to diversity in cortical synchronization levels (6, 87) and therefore patient- or region-specific diversity in time spent in the I-state versus the C-state. Our simulations indicate that different effect site concentrations of propofol tend to express different proportions of these two network states on a small spatial scale. Our results also suggest that, under propofol, different local cortical networks may, on a fast timescale, switch between the I-state and the C-state even while a regional EEG signal predominantly shows a single type of dose-dependent PAC. By introducing region-specific heterogeneity to cortex (e.g., sensory and higher order) and thalamus (e.g., core and matrix), future simulations may be able to investigate the significant spatiotemporal changes between low- and high-dose propofol. "Anteriorization" is a well-known phenomenon in which propofol administration initially leads to the loss of awake, occipital alpha and an increase in frontal alpha (13, 88, 89). This frontal alpha is at its strongest and most persistent state during low-dose propofol, before spreading to become region-nonspecific during high-dose propofol (3, 4, 7, 89) and decreasing in power with increasing dose (17). Slow power is also greater during high-dose than low-dose propofol (3, 4, 90, 91) and may modulate higher frequencies more in frontal regions during high dose (7). We note that our present modeling captures many of these results for frontal cortex: *1*) alpha is strongest and most persistent during low-dose propofol; *2*) alpha decreases in power with increasing dose; and *3*) slow power is greater during high-dose than low-dose propofol.

In the future, modeling multiple different areas of cortex will allow us to probe why holding propofol at a low dose results in trough-max coupling that is most prevalent in frontal cortex (4), why there is stronger frontal slow modulation at higher doses (7), and why there is increased thalamocortical alpha coherence in this region (50). Modeling multiple cortical areas will also allow us to explore coherence, phase (6), and firing rate (60) discrepancies found between frontal and sensory regions under anesthesia. Understanding how region-specific heterogeneity affects cross-cortical communication and frontal cortex specifically may help to validate theories of loss of consciousness, including frontoparietal disconnection (92) and similar connectivity changes (93), brain stem changes to neuromodulation (1), alpha blocking of processing (94), and slow oscillation control of activity (7, 95).

There is strong recent evidence that thalamic simulation can reverse unconsciousness during low-dose propofol (51). For our model to reproduce this, we would need to introduce additional mechanisms. One possible mechanism for this interesting phenomenon is that 30-s-long thalamic stimulation may activate group I metabotropic glutamatergic receptors (mGluRs) on the cortical cells receiving thalamocortical input. Thalamocortical activation of these receptors can produce depolarizing effects (96), and antagonism of cortical mGluRs leads to anesthesia-like effects (97). The very strong thalamocortical excitation elicited by thalamic stimulation may lead to activation of these mGluRs in the hyperpolarized cortical cells, depolarizing the cortical cells. This cortical depolarization could lead to a temporary reduction in cortical DOWN states (reducing SWO power) and an increase in higher-power activity. Conversely, since mGluRs also exist at corticothalamic synapses (29, 96), another contributor to the reversal of sedation could be that thalamic stimulation leads to thalamocortical excitation, which leads to corticothalamic stimulation that activates mGluRs, temporarily depolarizing the thalamus.

Propofol and Communication in the Thalamocortical Loop

Higher doses of propofol corresponding to increased colocalization of alpha and the peak of slow have been associated with unarousable consciousness, whereas lower doses of propofol with less peak-max colocalization lead to a state of unconsciousness in which arousability is possible (3–5). Our modeling suggests that the depth of anesthesia is associated with the degree of predominance of the I-state over the C-state. Since in our model cortical synchrony is a key driver of the transition from the C-state to the I-state and cortical desynchrony causes the opposite transition, our results suggest that increased cortical synchrony corresponds to deeper

levels of unconsciousness. This has also been noted in the experimental paper (98) on unconsciousness and synchrony in layer 5 cortical cells. Such increased synchronization prevents the flexible and fast changes of coordination needed for normal cognitive processing (99, 100).

Our model suggests that lower doses of propofol are associated with more time spent in the C-state. This state is associated with low-beta (as well as alpha) oscillations in the thalamus. As discussed above, beta oscillations have been documented to be highly involved in long-distance coordination in the brain (61). Thus, the loss of this beta could contribute to the higher degree of unconsciousness associated with higher doses.

One unintuitive finding suggested by our model was that TC neurons may be depolarized into "relay mode" during I-state and could potentially relay sensory information during this window, even during deep anesthesia. In our simulations, strong corticothalamic excitation after synchronized active cortical states increased the membrane potential of TC cells during the I-state, as shown in Fig. 3, *A* and *D*. This increase was enough to interrupt the intrinsic alpha bursts of the thalamus, but if this occurs at the same time as strong sensory input spikes the TC cells may be depolarized enough to briefly relay sensory spiking information up to the cortex. Recently, even in humans under low-dose propofol anesthesia, auditory stimuli resulted in wakelike cortical neural activity in primary auditory cortex but not higher-order cortex (60). This suggests that some thalamic sensory relay may still occur under propofol anesthesia, even if changes to cross-cortical communication prevent its higher-order processing. Furthermore, in our simulations, the I-state may occur during individual slow cycles of both low- and high-dose propofol, indicating that this brief sensory relay may occur at any point during propofol anesthesia (6, 60).

DATA AVAILABILITY

Data will be made available upon reasonable request.

SUPPLEMENTAL MATERIAL

Supplemental Data S1: https://doi.org/10.6084/m9.figshare.22228858.v1.

Supplemental Data S2: https://doi.org/10.6084/m9.figshare.22582312.v1.

ACKNOWLEDGMENTS

We thank the reviewers for helpful comments on a previous draft of this paper. We thank Jason Sherfey, Erik A. Roberts, Emily Stephen, and Caroline Moore-Kochlacs for suggestions during the investigation.

Present address of A. E. Soplata: École Polytechnique Fédérale de Lausanne, Blue Brain Project, Campus Biotech, Chemin des Mines 9, 1202 Geneva, Switzerland.

GRANTS

All authors were supported by NIH Grant P01GM118269 (to N.K. and E.N.B.). Other sources include Guggenheim Fellowship in Applied Mathematics (to E.N.B.), NIH R01-GM104948 (to E.N.B.), funds from Massachusetts General Hospital (to E.N.B.), and National Science Foundation DMS-1042134-5 (to N.K.).

DISCLOSURES

Massachusetts General Hospital has licensed intellectual property for EEG monitoring developed by E. N. Brown and P. L. Purdon to Masimo Corporation. P. L. Purdon and E. N. Brown have a financial interest in PASCALL Systems, Inc., a company developing closed-loop physiological control systems for anesthesiology. P. L. Purdon and E. N. Brown's interests were reviewed and are managed by Massachusetts General Hospital and Mass General Brigham in accordance with their conflict-of-interest policies. None of the other authors has any conflicts of interest, financial or otherwise, to disclose.

AUTHOR CONTRIBUTIONS

A.E.S., M.M.M., and N.K. conceived and designed research; A.E.S. performed experiments; A.E.S., E.A., M.M.M., and N.K. analyzed data; A.E.S., E.N.B., P.L.P., M.M.M., and N.K. interpreted results of experiments; A.E.S. and E.A. prepared figures; A.E.S., E.A., M.M.M., and N.K. drafted manuscript; A.E.S., E.A., E.N.B., P.L.P., M.M.M., and N.K. edited and revised manuscript; A.E.S., E.A., E.N.B., P.L.P., M.M.M., and N.K. approved final version of manuscript.

REFERENCES

1. **Brown EN**, **Purdon PL**, **Van Dort CJ.** General anesthesia and altered states of arousal: a systems neuroscience analysis. *Annu Rev Neurosci* 34: 601–628, 2011. doi:10.1146/annurev-neuro-060909-153200.
2. **Lewis LD**, **Weiner VS**, **Mukamel EA**, **Donoghue JA**, **Eskandar EN**, **Madsen JR**, **Anderson WS**, **Hochberg LR**, **Cash SS**, **Brown EN**, **Purdon PL.** Rapid fragmentation of neuronal networks at the onset of propofol-induced unconsciousness. *Proc Natl Acad Sci USA* 109: E3377–E3386, 2012. doi:10.1073/pnas.1210907109.
3. **Purdon PL**, **Pierce ET**, **Mukamel EA**, **Prerau MJ**, **Walsh JL**, **Wong KF**, **Salazar-Gomez AF**, **Harrell PG**, **Sampson AL**, **Cimenser A**, **Ching S**, **Kopell NJ**, **Tavares-Stoeckel C**, **Habeeb K**, **Merhar R**, **Brown EN.** Electroencephalogram signatures of loss and recovery of consciousness from propofol. *Proc Natl Acad Sci USA* 110: E1142–E1151, 2013. doi:10.1073/pnas.1221180110.
4. **Mukamel EA**, **Pirondini E**, **Babadi B**, **Wong KF**, **Pierce ET**, **Harrell PG**, **Walsh JL**, **Salazar-Gomez AF**, **Cash SS**, **Eskandar EN**, **Weiner VS**, **Brown EN**, **Purdon PL.** A transition in brain state during propofol-induced unconsciousness. *J Neurosci* 34: 839–845, 2014 [Erratum in *J Neurosci* 35: 8684–8685, 2015]. doi:10.1523/JNEUROSCI.5813-12.2014.
5. **Scheinin A**, **Kallionpää RE**, **Li D**, **Kallioinen M**, **Kaisti K**, **Långsjö J**, **Maksimow A**, **Vahlberg T**, **Valli K**, **Mashour GA**, **Revonsuo A**, **Scheinin H.** Differentiating drug-related and state-related effects of dexmedetomidine and propofol on the electroencephalogram. *Anesthesiology* 129: 22–36, 2018. doi:10.1097/ALN.0000000000002192.
6. **Malekmohammadi M**, **Price CM**, **Hudson AE**, **DiCesare JA**, **Pouratian N.** Propofol-induced loss of consciousness is associated with a decrease in thalamocortical connectivity in humans. *Brain* 142: 2288–2302, 2019. doi:10.1093/brain/awz169.
7. **Stephen EP**, **Hotan GC**, **Pierce ET**, **Harrell PG**, **Walsh JL**, **Brown EN**, **Purdon PL.** Broadband slow-wave modulation in posterior and anterior cortex tracks distinct states of propofol-induced unconsciousness. *Sci Rep* 10: 13701, 2020. doi:10.1038/s41598-020-68756-y.
8. **Gaskell AL**, **Hight DF**, **Winders J**, **Tran G**, **Defresne A**, **Bonhomme V**, **Raz A**, **Sleigh JW**, **Sanders RD.** Frontal alpha-delta EEG does not preclude volitional response during anaesthesia: prospective cohort study of the isolated forearm technique. *Br J Anaesth* 119: 664–673, 2017. doi:10.1093/bja/aex170.
9. **Brown EN**, **Lydic R**, **Schiff ND.** General anesthesia, sleep, and coma. *N Engl J Med* 363: 2638–2650, 2010. doi:10.1056/NEJMra0808281.
10. **Soplata AE**, **McCarthy MM**, **Sherfey J**, **Lee S**, **Purdon PL**, **Brown EN**, **Kopell N.** Thalamocortical control of propofol phase-amplitude coupling. *PLoS Comput Biol* 13: e1005879, 2017. doi:10.1371/journal.pcbi.1005879.

11. **Compte A**, **Sanchez-Vives MV**, **McCormick DA**, **Wang XJ.** Cellular and network mechanisms of slow oscillatory activity (<1 Hz) and wave propagations in a cortical network model. *J Neurophysiol* 89: 2707–2725, 2003. doi:10.1152/jn.00845.2002.
12. **Benita JM**, **Guillamon A**, **Deco G**, **Sanchez-Vives MV.** Synaptic depression and slow oscillatory activity in a biophysical network model of the cerebral cortex. *Front Comput Neurosci* 6: 64, 2012. doi:10.3389/fncom.2012.00064.
13. **Vijayan S**, **Ching S**, **Purdon PL**, **Brown EN**, **Kopell NJ.** Thalamocortical mechanisms for the anteriorization of alpha rhythms during propofol-induced unconsciousness. *J Neurosci* 33: 11070–11075, 2013. doi:10.1523/JNEUROSCI.5670-12.2013.
14. **Ching S**, **Cimenser A**, **Purdon PL**, **Brown EN**, **Kopell NJ.** Thalamocortical model for a propofol-induced alpha-rhythm associated with loss of consciousness. *Proc Natl Acad Sci USA* 107: 22665–22670, 2010. doi:10.1073/pnas.1017069108.
15. **Van Diepen RM**, **Foxe JJ**, **Mazaheri A.** The functional role of alpha-band activity in attentional processing: the current zeitgeist and future outlook. *Curr Opin Psychol* 29: 229–238, 2019. doi:10.1016/j.copsyc.2019.03.015.
16. **Foster JJ**, **Awh E.** The role of alpha oscillations in spatial attention: limited evidence for a suppression account. *Curr Opin Psychol* 29: 34–40, 2019. doi:10.1016/j.copsyc.2018.11.001.
17. **Gutiérrez R**, **Maldonado F**, **Egaña JI**, **Penna A.** Electroencephalographic alpha and delta oscillation dynamics in response to increasing doses of propofol. *J Neurosurg Anesthesiol* 34: 79–83, 2022. doi:10.1097/ANA.0000000000000733.
18. **Moody OA**, **Zhang ER**, **Vincent KF**, **Kato R**, **Melonakos ED**, **Nehs CJ**, **Solt K.** The neural circuits underlying general anesthesia and sleep. *Anesth Analg* 132: 1254–1264, 2021. doi:10.1213/ANE.0000000000005361.
19. **Soplata AE.** asoplata/soplata-2023-thalcort code. 2023. https://doi.org/10.5281/zenodo.7725212.
20. **Soplata AE.** DynaSim mechanism files for simulating thalamically-extended (Benita et al., 2012) slow wave model. 2023. https://doi.org/10.5281/zenodo.7725210.
21. **Destexhe A**, **Bal T**, **McCormick DA**, **Sejnowski TJ.** Ionic mechanisms underlying synchronized oscillations and propagating waves in a model of ferret thalamic slices. *J Neurophysiol* 76: 2049–2070, 1996. doi:10.1152/jn.1996.76.3.2049.
22. **Lytton WW**, **Destexhe A**, **Sejnowski TJ.** Control of slow oscillations in the thalamocortical neuron: a computer model. *Neuroscience* 70: 673–684, 1996. doi:10.1016/S0306-4522(96)83006-5.
23. **Sanchez-Vives MV**, **McCormick DA.** Cellular and network mechanisms of rhythmic recurrent activity in neocortex. *Nat Neurosci* 3: 1027–1034, 2000. doi:10.1038/79848.
24. **Timofeev I**, **Grenier F**, **Bazhenov M**, **Sejnowski TJ**, **Steriade M.** Origin of slow cortical oscillations in deafferented cortical slabs. *Cereb Cortex* 10: 1185–1199, 2000. doi:10.1093/cercor/10.12.1185.
25. **Bazhenov M**, **Timofeev I**, **Steriade M**, **Sejnowski TJ.** Model of thalamocortical slow-wave sleep oscillations and transitions to activated states. *J Neurosci* 22: 8691–8704, 2002. doi:10.1523/JNEUROSCI.22-19-08691.2002.
26. **Destexhe A**, **Sejnowski TJ.** Interactions between membrane conductances underlying thalamocortical slow-wave oscillations. *Physiol Rev* 83: 1401–1453, 2003. doi:10.1152/physrev.00012.2003.
27. **Hill S**, **Tononi G.** Modeling sleep and wakefulness in the thalamocortical system. *J Neurophysiol* 93: 1671–1698, 2005. doi:10.1152/jn.00915.2004.
28. **Crunelli V**, **Hughes SW.** The slow (<1 Hz) rhythm of non-REM sleep: a dialogue between three cardinal oscillators. *Nat Neurosci* 13: 9–17, 2010. doi:10.1038/nn.2445.
29. **Crunelli V**, **Errington AC**, **Hughes SW**, **Tóth TI.** The thalamic low-threshold Ca^{2+} potential: a key determinant of the local and global dynamics of the slow (<1 Hz) sleep oscillation in thalamocortical networks. *Philos Trans A Math Phys Eng Sci* 369: 3820–3839, 2011. doi:10.1098/rsta.2011.0126.
30. **Taxidis J**, **Mizuseki K**, **Mason R**, **Owen MR.** Influence of slow oscillation on hippocampal activity and ripples through cortico-hippocampal synaptic interactions, analyzed by a cortical-CA3-CA1 network model. *Front Comput Neurosci* 7: 3, 2013. doi:10.3389/fncom.2013.00003.
31. **Traub RD**, **Contreras D**, **Cunningham MO**, **Murray H**, **LeBeau FE**, **Roopun A**, **Bibbig A**, **Wilent WB**, **Higley MJ**, **Whittington MA.** Single-column thalamocortical network model exhibiting gamma oscillations, sleep spindles, and epileptogenic bursts. *J Neurophysiol* 93: 2194–2232, 2005. doi:10.1152/jn.00983.2004.
32. **Cruikshank SJ**, **Ahmed OJ**, **Stevens TR**, **Patrick SL**, **Gonzalez AN**, **Elmaleh M**, **Connors BW.** Thalamic control of layer 1 circuits in prefrontal cortex. *J Neurosci* 32: 17813–17823, 2012. doi:10.1523/JNEUROSCI.3231-12.2012.
33. **Krishnan GP**, **Chauvette S**, **Shamie I**, **Soltani S**, **Timofeev I**, **Cash SS**, **Halgren E**, **Bazhenov M.** Cellular and neurochemical basis of sleep stages in the thalamocortical network. *eLife* 5: e18607, 2016. doi:10.7554/eLife.18607.
34. **Ying SW**, **Abbas SY**, **Harrison NL**, **Goldstein PA.** Propofol block of I_h contributes to the suppression of neuronal excitability and rhythmic burst firing in thalamocortical neurons: propofol inhibition of thalamic I_h. *Eur J Neurosci* 23: 465–480, 2006 [Erratum in *Eur J Neurosci* 23: 1403, 2006]. doi:10.1111/j.1460-9568.2005.04587.x.
35. **Cacheaux LP**, **Topf N**, **Tibbs GR**, **Schaefer UR**, **Levi R**, **Harrison NL**, **Abbott GW**, **Goldstein PA.** Impairment of hyperpolarization-activated, cyclic nucleotide-gated channel function by the intravenous general anesthetic propofol. *J Pharmacol Exp Ther* 315: 517–525, 2005. doi:10.1124/jpet.105.091801.
36. **Chen X**, **Sirois JE**, **Lei Q**, **Talley EM**, **Lynch C 3rd**, **Bayliss DA.** HCN subunit-specific and cAMP-modulated effects of anesthetics on neuronal pacemaker currents. *J Neurosci* 25: 5803–5814, 2005. doi:10.1523/JNEUROSCI.1153-05.2005.
37. **McCarthy MM**, **Brown EN**, **Kopell N.** Potential network mechanisms mediating electroencephalographic beta rhythm changes during propofol-induced paradoxical excitation. *J Neurosci* 28: 13488–13504, 2008. doi:10.1523/JNEUROSCI.3536-08.2008.
38. **Kruglikov I**, **Rudy B.** Perisomatic GABA release and thalamocortical integration onto neocortical excitatory cells are regulated by neuromodulators. *Neuron* 58: 911–924, 2008. doi:10.1016/j.neuron.2008.04.024.
39. **Favero M**, **Varghese G**, **Castro-Alamancos MA.** The state of somatosensory cortex during neuromodulation. *J Neurophysiol* 108: 1010–1024, 2012. doi:10.1152/jn.00256.2012.
40. **Gil Z**, **Connors BW**, **Amitai Y.** Differential regulation of neocortical synapses by neuromodulators and activity. *Neuron* 19: 679–686, 1997. doi:10.1016/S0896-6273(00)80380-3.
41. **Hsieh CY**, **Cruikshank SJ**, **Metherate R.** Differential modulation of auditory thalamocortical and intracortical synaptic transmission by cholinergic agonist. *Brain Res* 880: 51–64, 2000. doi:10.1016/s0006-8993(00)02766-9.
42. **Oldford E**, **Castro-Alamancos MA.** Input-specific effects of acetylcholine on sensory and intracortical evoked responses in the "barrel cortex" in vivo. *Neuroscience* 117: 769–778, 2003. doi:10.1016/S0306-4522(02)00663-2.
43. **Eggermann E**, **Feldmeyer D.** Cholinergic filtering in the recurrent excitatory microcircuit of cortical layer 4. *Proc Natl Acad Sci USA* 106: 11753–11758, 2009. doi:10.1073/pnas.0810062106.
44. **Quick MW**, **Lester RA.** Desensitization of neuronal nicotinic receptors. *J Neurobiol* 53: 457–478, 2002. doi:10.1002/neu.10109.
45. **McCormick DA.** Neurotransmitter actions in the thalamus and cerebral cortex and their role in neuromodulation of thalamocortical activity. *Prog Neurobiol* 39: 337–388, 1992. doi:10.1016/0301-0082(92)90012-4.
46. **Vijayan S**, **Kopell NJ.** Thalamic model of awake alpha oscillations and implications for stimulus processing. *Proc Natl Acad Sci USA* 109: 18553–18558, 2012. doi:10.1073/pnas.1215385109.
47. **Kirschstein T**, **Köhling R.** What is the source of the EEG? *Clin EEG Neurosci* 40: 146–149, 2009. doi:10.1177/155005940904000305.
48. **Sherfey JS**, **Soplata AE**, **Ardid S**, **Roberts EA**, **Stanley DA**, **Pittman-Polletta BR**, **Kopell NJ.** DynaSim: a MATLAB toolbox for neural modeling and simulation. *Front Neuroinform* 12: 10, 2018. doi:10.3389/fninf.2018.00010.
49. **Babadi B**, **Brown EN.** A review of multitaper spectral analysis. *IEEE Trans Biomed Eng* 61: 1555–1564, 2014. doi:10.1109/TBME.2014.2311996.
50. **Flores FJ**, **Hartnack KE**, **Fath AB**, **Kim SE**, **Wilson MA**, **Brown EN**, **Purdon PL.** Thalamocortical synchronization during induction and emergence from propofol-induced unconsciousness. *Proc Natl Acad Sci USA* 114: E6660–E6668, 2017. doi:10.1073/pnas.1700148114.
51. **Bastos AM**, **Donoghue JA**, **Brincat SL**, **Mahnke M**, **Yanar J**, **Correa J**, **Waite AS**, **Lundqvist M**, **Roy J**, **Brown EN**, **Miller EK.**

Neural effects of propofol-induced unconsciousness and its reversal using thalamic stimulation. *eLife* 10: e60824, 2021. doi:10.7554/eLife.60824.

52. **Ching S**, **Purdon PL**, **Vijayan S**, **Kopell NJ**, **Brown EN.** A neurophysiological-metabolic model for burst suppression. *Proc Natl Acad Sci USA* 109: 3095–3100, 2012. doi:10.1073/pnas.1121461109.
53. **Kikuchi T**, **Wang Y**, **Sato K**, **Okumura F.** In vivo effects of propofol on acetylcholine release from the frontal cortex, hippocampus and striatum studied by intracerebral microdialysis in freely moving rats. *Br J Anaesth* 80: 644–648, 1998. doi:10.1093/bja/80.5.644.
54. **Nemoto C**, **Murakawa M**, **Hakozaki T**, **Imaizumi T**, **Isosu T**, **Obara S.** Effects of dexmedetomidine, midazolam, and propofol on acetylcholine release in the rat cerebral cortex in vivo. *J Anesth* 27: 771–774, 2013. doi:10.1007/s00540-013-1589-5.
55. **Meuret P**, **Backman SB**, **Bonhomme V**, **Plourde G**, **Fiset P.** Physostigmine reverses propofol-induced unconsciousness and attenuation of the auditory steady state response and bispectral index in human volunteers. *Anesthesiology* 93: 708–717, 2000. doi:10.1097/00000542-200009000-00020.
56. **Pal D**, **Mashour GA.** Consciousness, anesthesia, and acetylcholine. *Anesthesiology* 134: 515–517, 2021. doi:10.1097/ALN.0000000000003696.
57. **Luo TY**, **Cai S**, **Qin ZX**, **Yang SC**, **Shu Y**, **Liu CX**, **Zhang Y**, **Zhang L**, **Zhou L**, **Yu T**, **Yu SY.** Basal forebrain cholinergic activity modulates isoflurane and propofol anesthesia. *Front Neurosci* 14: 559077, 2020. doi:10.3389/fnins.2020.559077.
58. **Krishnan GP**, **González OC**, **Bazhenov M.** Origin of slow spontaneous resting-state neuronal fluctuations in brain networks. *Proc Natl Acad Sci USA* 115: 6858–6863, 2018. doi:10.1073/pnas.1715841115.
59. **Dash S**, **Autio DM**, **Crandall SR.** State-dependent modulation of activity in distinct layer 6 corticothalamic neurons in barrel cortex of awake mice. *J Neurosci* 42: 6551–6565, 2022. doi:10.1523/JNEUROSCI.2219-21.2022.
60. **Krom AJ**, **Marmelshtein A**, **Gelbard-Sagiv H**, **Tankus A**, **Hayat H**, **Hayat D**, **Matot I**, **Strauss I**, **Fahoum F**, **Soehle M**, **Boström J**, **Mormann F**, **Fried I**, **Nir Y.** Anesthesia-induced loss of consciousness disrupts auditory responses beyond primary cortex. *Proc Natl Acad Sci USA* 117: 11770–11780, 2020. doi:10.1073/pnas.1917251117.
61. **Siegel M**, **Donner TH**, **Engel AK.** Spectral fingerprints of large-scale neuronal interactions. *Nat Rev Neurosci* 13: 121–134, 2012. doi:10.1038/nrn3137.
62. **Weiner VS**, **Zhou DW**, **Kahali P**, **Stephen EP**, **Peterfreund RA**, **Aglio LS**, **Szabo MD**, **Eskandar EN**, **Salazar-Gomez AF**, **Sampson AL**, **Cash SS**, **Brown EN**, **Purdon PL.** Propofol disrupts alpha dynamics in functionally distinct thalamocortical networks during loss of consciousness. *Proc Natl Acad Sci USA* 120: e2207831120, 2023. doi:10.1073/pnas.2207831120.
63. **Jones SR**, **Pinto DJ**, **Kaper TJ**, **Kopell N.** Alpha-frequency rhythms desynchronize over long cortical distances: a modeling study. *J Comput Neurosci* 9: 271–291, 2000. doi:10.1023/a:1026539805445.
64. **Ujma PP**, **Szalárdy O**, **Fabó D**, **Erőss L**, **Bódizs R.** Thalamic activity during scalp slow waves in humans. *Neuroimage* 257: 119325, 2022. doi:10.1016/j.neuroimage.2022.119325.
65. **Wang D**, **Lipski WJ**, **Bush A**, **Chrabaszcz A**, **Dastolfo-Hromack CA**, **Dickey M**, **Fiez JA**, **Richardson RM.** Lateralized and region-specific thalamic processing of lexical status during reading aloud. *J Neurosci* 42: 3228–3240, 2022. doi:10.1523/JNEUROSCI.1332-21.2022.
66. **Silva LR**, **Amitai Y**, **Connors BW.** Intrinsic oscillations of neocortex generated by layer 5 pyramidal neurons. *Science* 251: 432–435, 1991. doi:10.1126/science.1824881.
67. **Bollimunta A**, **Mo J**, **Schroeder CE**, **Ding M.** Neuronal mechanisms and attentional modulation of corticothalamic alpha oscillations. *J Neurosci* 31: 4935–4943, 2011. doi:10.1523/JNEUROSCI.5580-10.2011.
68. **Sigala R**, **Haufe S**, **Roy D**, **Dinse HR**, **Ritter P.** The role of alpha-rhythm states in perceptual learning: insights from experiments and computational models. *Front Comput Neurosci* 8: 36, 2014. doi:10.3389/fncom.2014.00036.
69. **Lozano-Soldevilla D**, **Ter Huurne N**, **Oostenveld R.** Neuronal oscillations with non-sinusoidal morphology produce spurious phase-to-amplitude coupling and directionality. *Front Comput Neurosci* 10: 87, 2016. doi:10.3389/fncom.2016.00087.
70. **Köster M**, **Gruber T.** Rhythms of human attention and memory: an embedded process perspective. *Front Hum Neurosci* 16: 905837, 2022. doi:10.3389/fnhum.2022.905837.
71. **Jiang J**, **Zhao Y**, **Liu J**, **Yang Y**, **Liang P**, **Huang H**, **Wu Y**, **Kang Y**, **Zhu T**, **Zhou C.** Signatures of thalamocortical alpha oscillations and synchronization with increased anesthetic depths under isoflurane. *Front Pharmacol* 13: 887981, 2022. doi:10.3389/fphar.2022.887981.
72. **Schwindt PC**, **Spain WJ**, **Crill WE.** Long-lasting reduction of excitability by a sodium-dependent potassium current in cat neocortical neurons. *J Neurophysiol* 61: 233–244, 1989. doi:10.1152/jn.1989.61.2.233.
73. **Brown EN**, **Pavone KJ**, **Naranjo M.** Multimodal general anesthesia: theory and practice. *Anesth Analg* 127: 1246–1258, 2018. doi:10.1213/ANE.0000000000003668.
74. **Kuo MC**, **Dringenberg HC.** Histamine facilitates in vivo thalamocortical long-term potentiation in the mature visual cortex of anesthetized rats. *Eur J Neurosci* 27: 1731–1738, 2008. doi:10.1111/j.1460-9568.2008.06164.x.
75. **Minert A**, **Yatziv SL**, **Devor M.** Location of the mesopontine neurons responsible for maintenance of anesthetic loss of consciousness. *J Neurosci* 37: 9320–9331, 2017. doi:10.1523/JNEUROSCI.0544-17.2017.
76. **Minert A**, **Baron M**, **Devor M.** Reduced Sensitivity to anesthetic agents upon lesioning the mesopontine tegmental anesthesia area in rats depends on anesthetic type. *Anesthesiology* 132: 535–550, 2020. doi:10.1097/ALN.0000000000003087.
77. **Muindi F**, **Kenny JD**, **Taylor NE**, **Solt K**, **Wilson MA**, **Brown EN**, **Van Dort CJ.** Electrical stimulation of the parabrachial nucleus induces reanimation from isoflurane general anesthesia. *Behav Brain Res* 306: 20–25, 2016. doi:10.1016/j.bbr.2016.03.021.
78. **Vlasov K**, **Pei J**, **Nehs CJ**, **Guidera JA**, **Zhang ER**, **Kenny JD**, **Houle TT**, **Brenner GJ**, **Taylor NE**, **Solt K.** Activation of GABAergic neurons in the rostromedial tegmental nucleus and other brainstem regions promotes sedation and facilitates sevoflurane anesthesia in mice. *Anesth Analg* 132: e50–e55, 2021. doi:10.1213/ANE.0000000000005387.
79. **Sanchez-Vives MV**, **Nowak LG**, **McCormick DA.** Cellular mechanisms of long-lasting adaptation in visual cortical neurons in vitro. *J Neurosci* 20: 4286–4299, 2000. doi:10.1523/JNEUROSCI.20-11-04286.2000.
80. **Hage TA**, **Salkoff L.** Sodium-activated potassium channels are functionally coupled to persistent sodium currents. *J Neurosci* 32: 2714–2721, 2012. doi:10.1523/JNEUROSCI.5088-11.2012.
81. **Penagos H**, **Varela C**, **Wilson MA.** Oscillations, neural computations and learning during wake and sleep. *Curr Opin Neurobiol* 44: 193–201, 2017. doi:10.1016/j.conb.2017.05.009.
82. **Stickgold R.** Sleep-dependent memory consolidation. *Nature* 437: 1272–1278, 2005. doi:10.1038/nature04286.
83. **Galarza Vallejo A**, **Kroes MC**, **Rey E**, **Acedo MV**, **Moratti S**, **Fernández G**, **Strange BA.** Propofol-induced deep sedation reduces emotional episodic memory reconsolidation in humans. *Sci Adv* 5: eaav3801, 2019. doi:10.1126/sciadv.aav3801.
84. **Purdon PL**, **Pavone KJ**, **Akeju O**, **Smith AC**, **Sampson AL**, **Lee J**, **Zhou DW**, **Solt K**, **Brown EN.** The ageing brain: age-dependent changes in the electroencephalogram during propofol and sevoflurane general anaesthesia. *Br J Anaesth* 115: i46–i57, 2015. doi:10.1093/bja/aev213.
85. **Peters A.** Structural changes that occur during normal aging of primate cerebral hemispheres. *Neurosci Biobehav Rev* 26: 733–741, 2002. doi:10.1016/S0149-7634(02)00060-X.
86. **Morrison JH**, **Baxter MG.** The aging cortical synapse: hallmarks and implications for cognitive decline. *Nat Rev Neurosci* 13: 240–250, 2012. doi:10.1038/nrn3200.
87. **Redinbaugh MJ**, **Phillips JM**, **Kambi NA**, **Mohanta S**, **Andryk S**, **Dooley GL**, **Afrasiabi M**, **Raz A**, **Saalmann YB.** Thalamus modulates consciousness via layer-specific control of cortex. *Neuron* 106: 66–75.e12, 2020. doi:10.1016/j.neuron.2020.01.005.
88. **Tinker JH**, **Sharbrough FW**, **Michenfelder JD.** Anterior shift of the dominant EEG rhythm during anesthesia in the Java monkey: correlation with anesthetic potency. *Anesthesiology* 46: 252–259, 1977. doi:10.1097/00000542-197704000-00005.
89. **Cimenser A**, **Purdon PL**, **Pierce ET**, **Walsh JL**, **Salazar-Gomez AF**, **Harrell PG**, **Tavares-Stoeckel C**, **Habeeb K**, **Brown EN.** Tracking brain states under general anesthesia by using global coherence

analysis. *Proc Natl Acad Sci USA* 108: 8832–8837, 2011. doi:10.1073/pnas.1017041108.

90. **Mhuircheartaigh RN**, **Warnaby C**, **Rogers R**, **Jbabdi S**, **Tracey I.** Slow-wave activity saturation and thalamocortical isolation during propofol anesthesia in humans. *Sci Transl Med* 5: 208ra148, 2013. doi:10.1126/scitranslmed.3006007.
91. **Lee M**, **Sanders RD**, **Yeom SK**, **Won DO**, **Seo KS**, **Kim HJ**, **Tononi G**, **Lee SW.** Network properties in transitions of consciousness during propofol-induced sedation. *Sci Rep* 7: 16791, 2017. doi:10.1038/s41598-017-15082-5.
92. **Hudetz AG**, **Mashour GA.** Disconnecting consciousness: is there a common anesthetic end point? *Anesth Analg* 123: 1228–1240, 2016. doi:10.1213/ANE.0000000000001353.
93. **Banks MI**, **Krause BM**, **Endemann CM**, **Campbell DI**, **Kovach CK**, **Dyken ME**, **Kawasaki H**, **Nourski KV.** Cortical functional connectivity indexes arousal state during sleep and anesthesia. *NeuroImage* 211: 116627, 2020. doi:10.1016/j.neuroimage.2020.116627.
94. **Palva S**, **Palva JM.** New vistas for α-frequency band oscillations. *Trends Neurosci* 30: 150–158, 2007.doi:10.1016/j.tins.2007.02.001.
95. **Gemignani A**, **Menicucci D**, **Laurino M**, **Piarulli A**, **Mastorci F**, **Sebastiani L**, **Allegrini P.** Linking sleep slow oscillations with consciousness theories: new vistas on slow wave sleep unconsciousness. *Arch Ital Biol* 153: 135–143, 2015. doi:10.12871/000398292015238.
96. **Sherman SM.** The function of metabotropic glutamate receptors in thalamus and cortex. *Neuroscientist* 20: 136–149, 2014. doi:10.1177/1073858413478490.
97. **Suzuki M**, **Larkum ME.** General anesthesia decouples cortical pyramidal neurons. *Cell* 180: 666–676.e13, 2020. doi:10.1016/j.cell.2020.01.024.
98. **Bharioke A**, **Munz M**, **Brignall A**, **Kosche G**, **Eizinger MF**, **Ledergerber N**, **Hillier D**, **Gross-Scherf B**, **Conzelmann KK**, **Macé E**, **Roska B.** General anesthesia globally synchronizes activity selectively in layer 5 cortical pyramidal neurons. *Neuron* 110: 2024–2040.e10, 2022. doi:10.1016/j.neuron.2022.03.032.
99. **Cannon J**, **McCarthy MM**, **Lee S**, **Lee J**, **Börgers C**, **Whittington MA**, **Kopell N.** Neurosystems: brain rhythms and cognitive processing. *Eur J Neurosci* 39: 705–719, 2014. doi:10.1111/ejn.12453.
100. **Buzsáki G.** *Rhythms of the Brain* (Online). New York: Oxford University Press, 2009. https://doi.org/10.1093/acprof:oso/9780195301069.001.0001.